TECHNISCHE UNIVERSITÄT MÜNCHEN

Fakultät für Medizin

Klinik und Poliklinik für Plastische Chirurgie und Handchirurgie

Optimization of Scaffolds for the Delivery of Mesenchymal Stem Cells into Dermal Wounds

Elizabeth Ann Wahl, MSc

Vollständiger Abdruck der von der Fakultät für Medizin der Technischen Universität München zur Erlangung des akademischen Grades eines

Doktors der Naturwissenschaften

(Dr. rer. nat.)

genehmigten Dissertation.

Vorsitzende(r): Univ.-Prof. Dr. Carsten Schmidt-Weber

Prüfer der Dissertation:

1. Univ.-Prof. Dr. Hans-Günther Machens

2. Univ.-Prof. Dr. Johann Josef Hauner

Die Dissertation wurde am 17. Februar 2015 bei der Technischen Universität München eingereicht und durch die Fakultät für Medizin am 13. Mai 2015 angenommen.

ABSTRACT

The main obstacle to start the wound healing process in non-healing wounds is the lack of vasculature. Mesenchymal stem cells (MSCs) have been shown to promote tissue regeneration. They have also been used in combination with three-dimensional scaffolds as a promising approach in the field of regenerative medicine. The aim of this work was to (1) find a suitable dermal regenerative scaffold, from those already in use in clinics or under development, in which adipose-derived MSCs (AdMSCs) can form a synergistic relationship in order to assist in increasing wound healing potential and (2) further investigate one of the scaffolds to determine if the AdMSCs could be pre-conditioned in hypoxic-mimetic conditions with deferoxamine mesylate (DFO) to increase paracrine factor release in order to create a more stable and easier platform for culturing the cells in their native hypoxic conditions to deliver them to the wound bed. The tested scaffolds were based on chitosan, fibrin, bovine collagen with glycosaminoglycans (GAG), and decellularized porcine dermis, which were chosen due to their differences in the manufacturing procedure, origin, and protein composition. The cellular distribution, attachment, survival, metabolic activity, and paracrine release of the seeded cells were analyzed *in vitro* as well as the angiogenic effects *in vivo* using a chick chorioallantoic membrane (CAM) assay. From the four tested, the collagen-GAG scaffold was chosen for further investigation due to its promising results by way of factor release, scaffold compatibility, and *in vivo* performance. The optimal seeding density was determined, followed by hypoxic and paracrine factor release *in vitro* and *in vivo.* Furthermore, any effects of inflammation were analyzed in order to determine if there were negative effects on the delivery of the cells pre-conditioned in DFO by way of a collagen-GAG delivery vessel. In addition, through the CAM assay, the scaffold composition also influenced the angiogenic potential of AdMSCs *in vivo* where the collagen-GAG and fibrin based scaffolds showed the highest efficacy. Collagen-GAG scaffolds with AdMSCs pretreated with DFO could release higher levels of VEGF and SDF-1α than environmentally induced hypoxia *in vitro* and higher levels of VEGF *in vivo*. As environmentally induced hypoxia would not be feasible as treatment in clinical settings, the application of DFO to maintain the AdMSCs in a similar environment to their natural settings, which in turn increases their healing potential would create a more desirable option to bring MSCs a step closer to clinical application. This work provides valuable information to enhance wound healing by increasing angiogenesis in a scaffold-based approach, which is currently lacking when only the scaffold is utilized. Moreover, the pretreatment of the AdMSCs with DFO could further

increase the angiogenic potential of the cells while keeping them close to their natural oxygen tension and making it a more viable option for clinical translation.

Contents

NOMENCLATURE

2D	two-dimensional
3D	three-dimensional
AdMSC	adipose-derived mesenchymal stem cell
αMEM	alpha modified eagle's medium
bFGF	basic fibroblast growth factor
BMMSC	bone marrow-derived mesenchymal stem cell
CAM	chorioallantoic membrane
CCR2	c-c chemokine receptor 2
cDNA	complementary deoxyribonucleic acid
CD	cluster designation
CXCL	chemokine (C-X-C motif) ligand
CXCR4	chemokine (C-X-C motif) receptor
DAPI	4',6-diamidino-2-phenylindole
DFO	deferoxamine mesylate
DRT	dermal regeneration template
dsDNA	double stranded deoxyribonucleic acid
ECM	extracellular matrix
ELISA	enzyme-linked immunosorbent assay
FACS	fluorescence-activated cell sorting
FCS	fetal calf serum
FDA	food and drug administration
GAG	glycosaminoglycan
GvHD	graft versus host disease
HIF	hypoxia inducible factor
HLA-DR	human leukocyte antigen-D related
HUVECs	human umbilical vein endothelial cells
IFN	interferon
IL	interleukin
LDH	lactate dehydrogenase
MCP	monocyte chemoattractant protein
MIF	macrophage migration inhibitory factor
MMP	metalloproteinase
MSC	mesenchymal stem cell
N	biological replicate
n	technical replicate
p	probability
P/S	penicillin/streptomycin

PBS	phosphate buffered saline
PlGF	placental growth factor
PLB	passive lysis buffer
RNA	ribonucleic acid
ROS	reactive oxygen species
RT-PCR	reverse transcription polymerase chain reaction
SDF	stromal cell-derived factor
SEM	scanning electron microscopy
SVF	stromal vascular fraction
TNF	tumor necrosis factor
VEGF	vascular endothelial growth factor

LIST OF FIGURES AND TABLES

1. INTRODUCTION

As the largest organ in the body, skin is in a constant state of change by shedding and replacing cells. It is important for immune function, regulating body temperature, vitamin adsorption, and sensation. Therefore, the function of the tissue is just as important as the formation. As skin is very complex, containing cells, sweat glands, hair follicles, sebaceous glands, and blood vessels, it can never fully regenerate, but it can heal to resemble healthy skin as is necessary for basic functioning.

Wound healing under physiological conditions consists of three steps: inflammation, proliferation, and maturation (Fig. 1). The initial inflammatory stage usually lasts three days. During the proliferative stage, new blood vessels begin to form and cover the wound together with the reconstruction and epithelialization of the wound which can take up to 4 weeks. The last stage of maturation and remodeling can continue for up to two years. In the case of diabetics, immunologically impaired, or elderly patients, complications can arise resulting in chronic non-healing wounds that cannot get past the initial stage of inflammation and require medical intervention. As is the case for third-degree burn victims, where all layers of the skin are damaged and, therefore, cannot regenerate, whereas superficial burns normally heal within 14 days.

Non-healing chronic wounds, such as venous leg ulcers, diabetic foot ulcers, and pressure ulcers, have a major impact on the healthcare system. In the US, these problems effect more than 8 million people with annual costs around $20 billion (Brem et al., 2010). With an aging population and a likelihood that the majority of the costs come from patients over 65, the costs could increase (Gould et al., 2014). In addition, these wounds have a negative effect on the quality of life of the patients (Barrientos et al., 2014; Hopman et al., 2009) as well as diabetic related amputations (Golinko et al., 2009; Moulik et al., 2003) and mortality rates of 68% from advanced pressure ulcers (Brown, 2003).

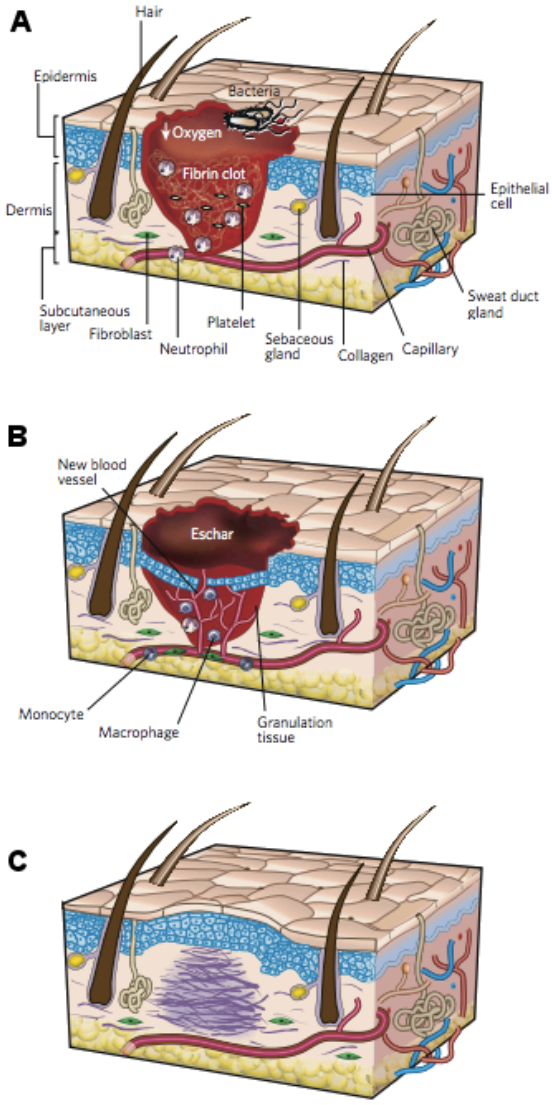

Figure 1. The three classic stages of wound repair include inflammation (A), proliferation (B), and maturation (C). Adapted from (Gurtner et al., 2008).

Due to the lack of functional recovery during the healing process, transplantation of autologous or allogeneic healthy tissue, also known as split-thickness skin grafts, developed in the 1960s, has become the "gold standard" in clinical treatments. A split-thickness skin graft involves the removal of the epidermis and part of the dermis from any healthy part of a donor's body, which is then transplanted to a wounded area. In many cases, a sufficient amount of healthy tissue may not be available from the donor in need of an autologous skin graft. On the other hand, an allogeneic transplant poses the risk of disease transmission or donor rejection. To address issues such as these, dermal regenerative substitute biomaterials have been developed to increase healing which are used in clinics worldwide. The general idea of these biomaterials is to mimic the extracellular matrix (ECM) in order to make it easier for cells to migrate and differentiate (chapter 1.2). One of the main issues of these materials with healing is the slow rate of angiogenesis. Thus, the induction of therapeutic vascularization is a major topic of research in the field of regenerative medicine. In order to increase angiogenesis, growth factors have been administered but they are costly and have a short half-life. A natural additive, such as mesenchymal stem cells (chapter 1.3) has been proposed to bridge this gap, which could increase the rate of angiogenesis and in turn help in more efficient wound healing.

1.1 Mesenchymal Stem Cells

In 1867, Julius Cohnheim published his work in which he found what later came to be known as mesenchymal stem cells (MSCs) located in bone marrow (BM) and proposed that these cells can migrate and regenerate injured tissue (Cohnheim, 1867). Almost a century later, Alexander Friedenstein, *et al.* isolated and exhibited that these cells could differentiate (Friedenstein et al., 1966). Since their pioneering work, MSCs have been found to exist in nearly every adult tissue (bone marrow, adipose tissue, skin, brain, liver, dental pulp, cornea, umbilical cord blood, placenta, amniotic fluid, and blood vessels) (Akpinar et al., 2014; Atala et al., 2012; Branch et al., 2012; Chen et al., 2014; da Silva Meirelles et al., 2006; Steigman and Fauza, 2007) and may originate from totipotent embryonic neural crest cells (Achilleos and Trainor, 2012).

Human MSCs have been recently defined as those that have plastic adherence in standard cell culture conditions, express the surface molecules CD105 (endoglin), CD73 (5' nucleotidase), and CD90 (Thy-1) while lacking the expression of CD45 (pan-hematopoietic SC), CD34 (endothelial and hematopoietic), CD14 (macrophage) or CD11b (leukocyte), CD79α or CD18 (B-cells), and HLA-DR (stimulated MSCs), and are able to differentiate into osteoblasts, adipocytes, and chondrocytes (Dominici et al., 2006). Although, to date, there are no known unique surface molecules to distinguish MSCs from a heterogeneous cell population and when they are grown in culture the expression of the molecules may change (Locke et al., 2009).

MSCs have been used in various studies in order to enhance tissue regeneration. Clinical data describes their beneficial regenerative effects in several organs and tissues, such as, the heart, cornea, nerves, bone, and skin (Bieback et al., 2012; Maxson et al., 2012; Mizuno et al., 2012; Zomorodian and Baghaban Eslaminejad, 2012). In order to administer MSCs to patients, cells have been introduced systemically and locally. While MSCs do have a homing capability to migrate to injured tissue, it has been described that after systemic administration, only a fraction of the cells can migrate to the target tissue, while the majority of cells accumulate at the kidney and lungs (Barbash et al., 2003; Chavakis et al., 2008; Kang et al., 2012). Pretreatment of the cells with heparin has been introduced in order to increase the number of cells making their way to the injured tissue (Yukawa et al., 2012). In the case of local injections, a large number of cells are required and, while an important

fraction of the cells remain in the area, another part is flushed out to the blood circulation (Bieback et al., 2012; Pittenger, 1999).

Engrafted MSCs can release a series of cytokines and growth factors by interacting with local tissue to enhance repair and regeneration (Kang et al., 2012; Ma et al., 2014). Recent studies support the idea that MSCs modulate the regenerative microenvironment by the controlled release of several paracrine factors related to key processes such as angiogenesis, cell homing, immunomodulation, tissue remodeling, and fibrosis (Anthony and Shiels, 2013; Baraniak and McDevitt, 2010; Reagan and Kaplan, 2011). Thus, MSCs may impact regeneration primarily by releasing paracrine factors necessary in wound healing (Broughton et al., 2006; Chen et al., 2008; Newman et al., 2009; Singer and Caplan, 2011; Yew et al., 2011) rather than by tissue replacement.

1.1.1 Adipose derived Mesenchymal Stem Cells

Adipose derived MSCs (AdMSCs) came into light as a stem cell source in 1992 from porcine tissue (Young et al., 1992). They are easily obtained from the stromal vascular fraction (SVF) (Zuk et al., 2002), which can be acquired from what is normally discarded medical waste from superficial fat removal surgeries and, therefore, do not require excess or risky procedures. The SVF contains a variety of cells, including endothelial cells, smooth muscle cells, pericytes, fibroblasts, as well as leucocytes, hematopoietic stem cells, and endothelial progenitor cells (Tholpady et al., 2006). These cells do not adhere to tissue culture plastic and can be removed through subsequent passaging, leaving a more homogeneous population of cells *in vitro* (Ogawa, 2006). Alternatively, magnetic activated cell sorting can be utilized in order to remove CD45+ and CD31+ cells (Boquest et al., 2005).

As bone marrow was the first source of MSCs discovered, several of the early studies focused on their utilization. Today, some advantages have been seen from using other sources. For instance, the age of the AdMSC donor does not affect their proliferation rate or differentiation potential as it does with bone marrow derived MSCs (BMMSCs) (Chen et al., 2012; Harris et al., 2010; Mirsaidi et al., 2012). This gives AdMSCs the potential to be used in an autologous manner in elderly patients in regenerative medicine. Furthermore, as the growth medium substitute, fetal calf serum (FCS), should

be limited if the cells are intended to be used in a clinical setting, human serum would make a more appropriate substitute as AdMSCs have shown superior adhesion and expansion when human serum was used (Pawitan, 2011).

A high quantity of MSCs can be obtained from a small amount of fat tissue. At least one million AdMSCs can be obtained from just 200 ml (~2% of total cell count) of lipoaspirates with more than 90% viability and virtually no harm to the donor. Whereas, only about 40 ml of aspirate, at most, can be taken from bone marrow at a time without risking donor site morbidity, which only contains 0.01-0.001% of MSCs of the total cell count from the entire aspirate (Aust et al., 2004; Pittenger, 1999; Strem et al., 2005). Furthermore, as vasculature is believed to be rich in MSCs, it is not surprising that a large quantity of AdMSCs can be isolated from a small amount of adipose tissue, which is highly vascularized (Crandall et al., 1997; Lin et al., 2010).

Several studies have shown the immunosuppressive properties of AdMSCs which lack human leukocyte antigen class II (HLA-DR) and are, furthermore, suppressed through inhibition of soluble factors, such as prostaglandin E2, nitric oxide, indoleamine 2,3-dioxygenase, interleukin (IL)-6, heme oxygenase-1, and human leukocyte antigen-G (Bouffi et al., 2010; Chabannes et al., 2007; Ren et al., 2008; Sato et al., 2007; Selmani et al., 2008; Spaggiari et al., 2008; Yang et al., 2012). This has allowed for xenogeneic transplantation into immunocompetent recipients for various disease models showing significant improvement without suppressing the immune system (Lin et al., 2012; Lin et al., 2010). Furthermore, clinical and preclinical studies have shown that allogeneic transplants of AdMSCs do not result in graph-versus-host disease (GvHD) and have been used to treat GvHD after hematopoietic stem cell transplantation (Baron and Storb, 2012; Kim et al., 2013; Lin et al., 2012).

1.1.2 MSC Niche and Hypoxia

The specialized microenvironment or niche of stem cells *in vivo* was first formally suggested in 1978 by Raymond Schofield (Schofield, 1978) and later clarified as the natural anatomical environment that contains cells and other components, such as blood vessels and matrix glycoproteins, balanced by the signaling of local cues to regulate self-renewal and differentiation (Mohyeldin et al., 2010; Muscari

et al., 2013). Furthermore, low oxygen tensions detected in developing embryos in 1968 (Mitchell and Yochim, 1968) later brought into question the oxygen tension of adult tissues and those known to harbor stem cells were found to have even lower oxygen tensions. These low oxygen conditions help stem cells retain their undifferentiated state, proliferate, and promote self-renewal (Mohyeldin et al., 2010). Although adipose tissue is highly vascularized, the tissue itself harbors a low oxygen tension, generally less than 3% O_2 (Matsumoto et al., 2005; Mohyeldin et al., 2010; Yamamoto et al., 2013) (Fig. 2).

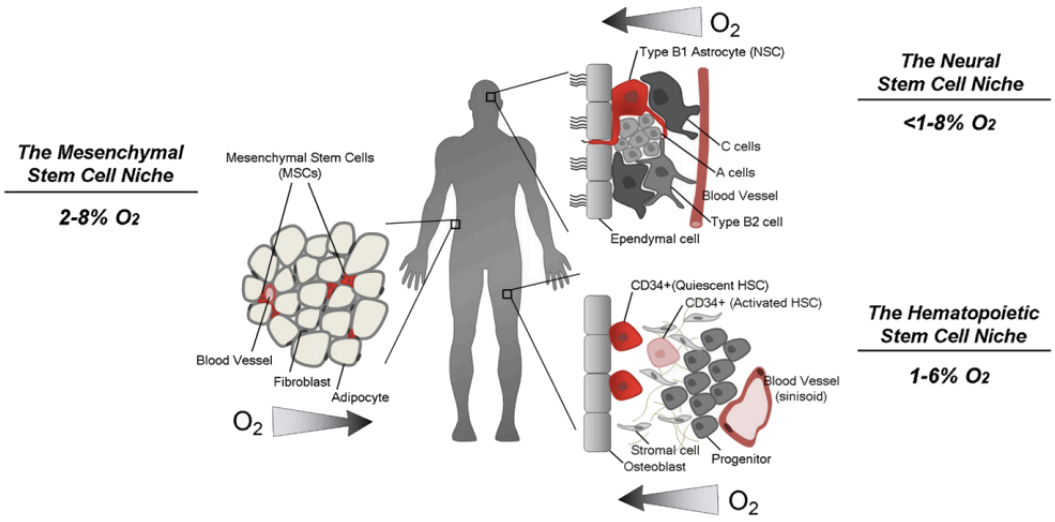

Figure 2. Oxygen tension in stem cell niches Bone marrow, adipose tissue, and the subventrical zone are rich in hematopoietic (Chow et al., 2001; Cipolleschi et al., 1993; Eliasson and Jonsson, 2010; Grant and Root, 1947), mesenchymal (Harrison et al., 2002; Kofoed et al., 1985; Matsumoto et al., 2005; Pasarica et al., 2009), and neural stem cells (Dings et al., 1998; Erecinska and Silver, 2001; Panchision, 2009), respectively. Low oxygen tensions have been found in all of three of these areas where the stem cells reside. Graphic adapted from (Mohyeldin et al., 2010).

The rate of proliferation and expression of anti-inflammatory markers from AdMSC increases when they are exposed to hypoxic preconditioning *in vitro.* Pretreatment in low oxygen culture conditions or chemically induced hypoxia-mimetic conditions of MSCs can make them more resistant to death when grafted to injured tissue (Muscari et al., 2013). MSCs preconditioned in hypoxic conditions and then transplanted *in vivo* have been found to lead to enhanced revascularization and angiogenesis in the hind limb ischemia model (Rosova et al., 2008; Yu et al., 2013).

Hypoxia inducible factor (HIF) is a heterodimeric transcription factor with both α and β subunits responsible for cell adaptation to hypoxia. At oxygen levels below 5%, HIF levels will increase (Pouyssegur et al., 2006). HIF-1α, the best described subunit, is degraded under normoxic conditions and stabilized under low oxygen tensions and hypoxia-mimetic conditions (Zagorska and Dulak, 2004). The stabilization of HIF-1α increases cell survival and upregulates growth factor secretion, which, in turn, increases angiogenesis, wound healing, and anti-apoptosis effects (Chung et al., 2009; Kaufman, 2010; Muscari et al., 2013; Takubo et al., 2010; Yu et al., 2013) (Fig. 3).

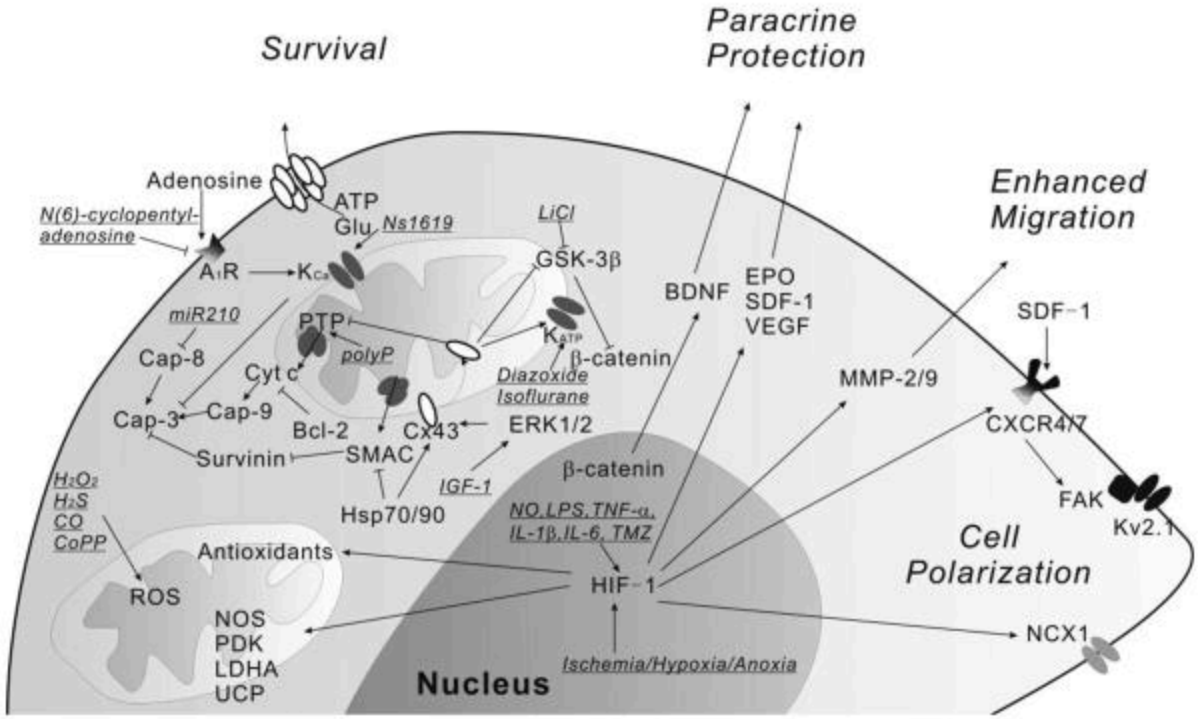

Figure 3. Functional aspects of HIF-1 MSCs preconditioned with hypoxia or hypoxia-mimetic conditions express hypoxia inducible factor (HIF)-1, which promotes survival, migration, paracrine release, and cell polarization making it an optimal treatment for cell transplantation therapy. Graphic adapted from (Yu et al., 2013).

Increased levels of HIF-1α in MSCs upregulate potent angiogenic factors, such as vascular endothelial growth factor (VEGF) and CXCR4, a stem cell surface chemokine receptor for stromal cell-derived factor (SDF)-1α (Hung et al., 2007; Schioppa et al., 2003; Yu et al., 2013; Zhao et al., 2008). VEGF is vital for wound healing and promotes new vessel growth by stimulating endothelial cell migration and division. SDF-1α is a critical factor for MSC migration, adhesion, and survival (Liu et al., 2010). Repressing HIF in diabetic mouse wounds has been shown to suppress VEGF and SDF-

1α and induce hyperglycemia, effectively delaying wound healing (Botusan et al., 2008). This indicates that the suppression of HIF-1α corresponds to a suppression of angiogenesis, which in turn impairs wound healing.

1.1.2 Deferoxamine mesylate induces hypoxia in MSCs

Deferoxamine mesylate (DFO), an FDA-approved iron chelating agent, can induce hypoxia mimetic conditions by stabilizing HIF-1α (Hirsila et al., 2005). DFO has been shown to increase the homing of BMMSCs as well as increase chemokine receptors CXCR4 and CCR2 and matrix metalloproteinases (MMP)-2 and -9 by stabilizing HIF-1α *in vitro* and *in vivo* (Najafi and Sharifi, 2013). Furthermore, DFO has been shown to increase angiogenic factors, VEGF and bFGF (Potier et al., 2008) as well as increase collagen density (Duscher et al., 2015).

Reactive oxygen species (ROS) production in wounds creates a hypoxic environment in the wound bed (Castilla et al., 2012). While the existence of some ROS, such as mitochondrial ROS, has been found to be vital to promote wound healing (Xu and Chisholm, 2014), excessive production can cause damage to DNA, RNA, and proteins, as well as induce apoptosis. Treatment of wounds with DFO has shown a decrease in ROS production (Bartolome et al., 2009; Basaran et al., 2013), which may help contribute to the positive outcome that has been seen in research thus far utilizing DFO.

1.2 Biological Scaffolds for Dermal Regeneration

Integra® Dermal Regeneration Template (DRT) was the first dermal substitute, created in 1979, by surgeon Dr. John F. Burke and mechanical engineer, Dr. Ioannas Yannas (Burke et al., 1981). It consists of bovine collagen crosslinked by chondroitin-6-sulphate glycosaminoglycans (GAGs) with a protective silicone membrane. Integra® DRT was designed to facilitate healing of the dermal layer. While Integra® DRT are void of living organisms, there are dermal regenerative substitutes, such as Dermagraft® which contain living human fibroblasts. Both of these scaffolds have been shown to improve healing of the wounded area although Integra® DRT is only applied once and biodegradable while Dermagraft® needs several applications for the fibroblasts to be effective.

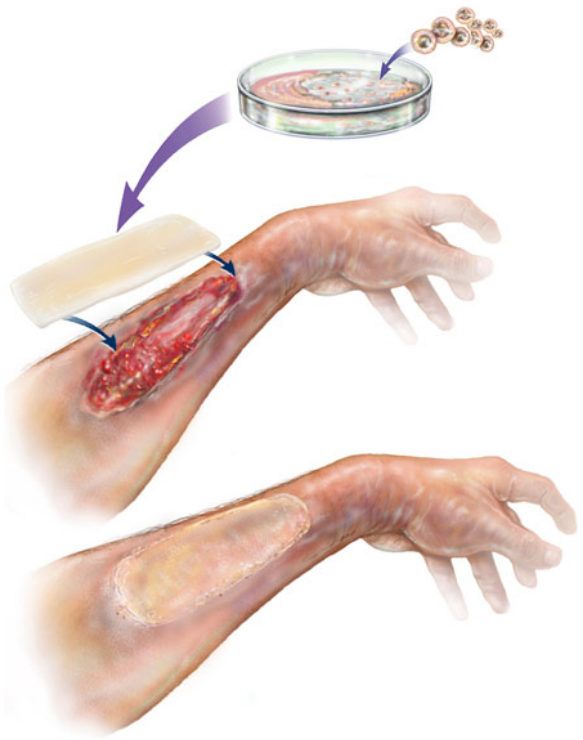

Figure 4. Scaffold guided wound healing activated with mesenchymal stem cells
Adapted from (PTEI, 2014).

A number of materials are being utilized and tested in clinics worldwide for wounds made from synthetic polymers, naturally derived materials, xenographic tissue, or a combination of different elements. As already mentioned, some may even contain cells. Several have been fabricated to mimic materials, from individual components of the extracellular matrix (ECM), such as collagen, fibronectin, or hyaluronic acid (Chattopadhyay and Raines, 2014; Collins and Birkinshaw, 2013; Halbleib et al., 2003; Seidlits et al., 2011), alone or in combination with each other as well as completely decellularized xenographic or human ECM from porcine small intestine mucosa and human placenta, respectively (Choi et al., 2013; Sun et al., 2013). Other materials have been used in combination with these ECM components, such as chitosan and alginate (Kim et al., 2014; Lauto, 2009), to improve wound healing.

All scaffolds, independent of the material, need to be able to mimic the natural environment of the ECM in the wound bed to provide optimal conditions for healing. Furthermore, they must be biocompatible in order to avoid inflammation of the surrounding tissue, degradable, be able to mimic the mechanical properties similar at the insertion site, and support cell interaction to facilitate regeneration, while reducing infection and scar tissue (Atala et al., 2012).

As the cells, blood vessels, 3D space, matrix glycoproteins, and glands make up the microenvironment in skin, a scaffold alone will only generate moderate results. The ECM, making up a majority of the dermal layer, alone consists of too many components to accurately be recreated in a synthetic form (Atala et al., 2012). The addition of MSCs could strengthen the outcome of chronic wounds by increasing release of paracrine factors and rates of angiogenesis.

1.3 MSC Scaffold Bioactivation

Different types of biomaterials are widely used to directly administer MSCs into wounds and to facilitate the healing process. For instance, fibrin sprays and microbeads have been used for chronic skin wounds (Falanga et al., 2007; Kirsner et al., 2013; Xie et al., 2013b), while meshes and 3D scaffolds have been used to treat ischemic heart tissue (Xing et al., 2012) and diabetic ischemic ulcers (Hou et al., 2013a). Different products on the market have received FDA approval and the development of new materials is ongoing in order to deal with the various forms of chronic wounds and tissue defects. These scaffolds vary in key parameters such as thickness, material composition, porosity, roughness, price, and availability. In order to increase the healing potential of scaffolds and of MSCs, they have been combined to enhance the regenerative potential of the scaffold and increase the retention rate of the MSCs (Fig. 4). Furthermore, the scaffolds need to make cells feel as if they are in their natural environment.

MSCs may impact regeneration primarily by releasing paracrine factors necessary in wound healing rather than by tissue replacement (Broughton et al., 2006; Chen et al., 2008; Newman et al., 2009; Singer and Caplan, 2011; Yew et al., 2011). As a result, the application of AdMSC seeded scaffolds to wounds could be beneficial in all of the three phases of wound healing: inflammation, proliferation, and tissue remodeling.

2. MOTIVATION

As AdMSCs can be obtained easily, proliferate quickly, and have the same characteristics as the current stem cell definition, their use for clinical applications would be desirable. Several studies have proposed the combined use of scaffolds for dermal regeneration with stem cells for the treatment of chronic skin ulcers. In those studies, it has been shown that after seeding, the cells are able to survive in the scaffolds, releasing several bioactive molecules that enhance skin regeneration *in vivo* [7, 21-23]. Although results are robust in preclinical trials, several issues have to be clarified and optimized before clinical translation. In the case of chronic wounds, the cells must secrete optimal amounts of paracrine factors in order to meet the demand necessary for healing. The addition of MSCs from a healthy donor into the scaffold should support the healing process by creating a pro-regenerative microenvironment in the wound area. The key issue of determining the best combination of cells with a material and the development of an optimized composite material with increased regenerative capacity remains to be addressed.

For cell survival and tissue function to persist, angiogenesis is a requirement. As synthesized growth factor delivery has a short half-life, a therapeutic promotion of angiogenic factor release would help create a more reliable, accelerated rate of healing for patients. In addition, if the cells could be preconditioned in low oxygen, as they exist in their niche and the environment of the wound bed, their healing potential should increase. As an environmental hypoxia incubator is inconvenient in a clinical setting, the addition of chemically induced hypoxia-mimetic conditions could possibly stabilize the cells, as in their niche, and provide a translational step towards clinical use of AdMSCs in a scaffold based approach to wound healing.

For this work, the structure consists of (1) investigation of the relationship of commercially used and pending for use dermal regenerative scaffolds, chosen for their current use in clinics as well as difference in material and structure, and AdMSCs to attach and release adequate growth factors *in vitro* and the angiogenic potential of the release *in vivo* (chapter 4.1), (2) the further investigation of the influence of hypoxia and hypoxia-mimetic conditions of the AdMSCs *in vitro* on one of the dermal regenerative scaffolds that shows the best potential for increased angiogenesis (chapter 4.2), and (3)

the evaluation of the optimized hypoxia and hypoxia-mimetic conditions in an *in vivo* mouse model to improve wound healing by way of increased angiogenesis (chapter 4.3).

3. MATERIALS AND METHODS

3.1 AdMSC Isolation and Characterization

3.1.1 Cell isolation and culture

Adipose tissue was derived from lipoaspirates obtained from donors who underwent fat removal for medical or aesthetic reasons and had given informed consent to participate in the study. The tissue was added to 50 ml Falcon tubes and an equal volume of 0.3 U/ml collagenase A (Roche, Basel, Switzerland) was added. The tissues were then incubated for 30 min at 37°C. After centrifugation, the resulting stromal vascular fraction was plated under standard conditions in Alpha Modified Eagle's Medium with nucleosides and 2.0 g/l $NaHCO_3$ (αMEM; Biochrom, Berlin, Germany), supplemented with 10% fetal calf serum (FCS; PAA, Pasching, Austria), and 1% penicillin/streptomycin (P/S; Biochrom) under standard cell culture conditions (37°C, 5% CO_2). In all experimental settings, cells from passages 3 were used with three donors (N = 3) and performed in triplicate (n = 3).

3.1.2 Cell characterization

AdMSCs were exposed to supplemented medium to differentiate into osteoblasts, adipocytes, and chondrocytes (n = 3, N = 3). The effectiveness was tested by staining and gene expression analysis. Cells exposed to adipogenic and osteogenic differentiation medium were seeded in 6 well plates for staining and 12 well plates for gene expression analysis. Cells exposed to chondrogenic medium were pelleted in 15 ml falcon tubes.

3.1.2.1 Staining

To test the osteogenic differentiation potential of the AdMSCs, 3,100 cells per cm^2 were seeded and allowed to reach 80-90% confluency before induction. Then either control medium (αMEM with 10% FCS and 1% P/S) or osteogenic medium (hMSC osteogenic differentiation BulletKit™, Lonza, Basel, Switzerland) was used to induce osteoblast growth. Medium was changed every 3-4 days. After 21 days in culture, cells were fixed with 10% v/v formalin solution for 15 min, rinsed with phosphate

buffered saline (PBS; Biochrom), stained with 0.5% w/v Alizarin Red S indicator (Ricca Chemicals Company, Arlington, TX) for 30 min with gentle shaking, washed 3 times with PBS, and imaged for calcium deposition.

To test the adipogenic differentiation of AdMSCs, cells were seeded at a density of 21,000 cells per cm^2 until they reached 80-90% confluence. Medium was then changed to either control medium (αMEM with 10% FCS and 1% P/S) or adipogenic induction medium (hMSC adipogenic differentiation BulletKit™, Lonza). Medium changes alternated between induction and maintenance medium following manufacturer's instructions. Cells were fixed after 25 d in culture with 10% v/v formalin solution, rinsed with PBS, and stained with Oil Red O (Electron Microscopy Sciences, Hatfield, PA), washed 3 times with PBS, and the resulting adipocytes were imaged (Nikon Eclipse TS100 Inverted Microscope).

Chondrogenic differentiation potential was carried out with three-dimensional pellet cultures initially formed by centrifugation in 15 ml polypropylene conical tubes. The initial pellets contained 2.5×10^5 cells and were cultivated for 21 d in either control medium or chondrogenic induction medium (hMSC chondrogenic differentiation BulletKit™, Lonza) supplemented with TGF Beta 3 (Lonza). Each medium changed for experimental cells contained fresh TGF Beta 3. After collection, pellets were rinsed with PBS and fixed in formalin. Pellets were either paraffin embedded and sectioned (5 µm) or left intact and stained with Alcian Blue to visualize acetic mucins and acid mucosubstances then further counterstained with Nuclear Fast Red (both from Sigma-Aldrich, St. Louis, MO, USA). All stainings were carried out with an n = 3 and N = 3.

3.1.2.2 Fluorescence-assisted cell sorting MSC surface marker characterization

For analysis of cell surface markers by flow cytometry, AdMSCs were detached from the culture flasks with trypsin-EDTA solution (Biochrom), rinsed with PBS, and incubated for 45 min with Phycoerythrin (PE)-conjugated antibodies raised against CD45, CD73, CD90, CD105, and CD146 at 4°C (1:100 dilution) (n = 3, N = 3). As isotype controls, IgG-PE was used (all antibodies from BD

Biosciences, San Jose, CA). Samples were examined with a Cytomics FC500 (Beckman Coulter, Brea, CA) (FACS analysis performed by Fernando Fierro).

3.2 Scaffold Characterization and Cell Seeding

Four scaffolds, based on different biomaterials, were tested in this study. Here we compared a chitosan film (BioPiel®), fibrin matrix (Smart Matrix™), collagen-GAG matrix (Integra® DRT), and decellularized dermis (Strattice™). BioPiel® (Recalcine, Santiago, Chile) is a commercially available wound dressing with hemostatic and bacteriostatic properties composed of chitosan. Smart Matrix™ (RAFT, Northwood, Middlesex, UK) is a porous crosslinked fibrin-alginate composite biomaterial developed at the RAFT Institute and is not yet commercially available. Integra® DRT (Integra Life Sciences, Plainsboro, NJ, USA) is a commonly used, FDA approved, biodegradable porous scaffold based on bovine type I collagen fibers that are crosslinked by glycosaminoglycans with a protective silicon layer. Strattice™ (LifeCell Corporation, Branchburg, NJ, USA) is an FDA approved porcine decellularized dermal matrix. In all experiments, 6 mm (in diameter) discs of scaffold, as created with a biopsy punch, were used.

3.2.1 Structural analysis of the scaffolds

The micro- and macrostructures of the scaffolds were analyzed by scanning electron microscopy (SEM) and a stereomicroscope, respectively. Scaffolds were dehydrated with graded ethanol, air-dried, and sputter coated with gold for 80 sec at 40 mA (Sputter Coating Device SCD 005, Bal-Tec AG, Liechtenstein). Analysis was performed at 5 kV accelerating voltage in a scanning electron microscope (SEM; Jeol JSM-5400, Japan). For macro analysis, scaffolds were imaged using a stereoscope (Zeiss, Jena, Germany) from the side and top view. SEM performed by Ursula Hopfner.

3.2.2 Cell seeding on scaffolds

Scaffolds were placed in 24-well plates and 1.8×10^5 AdMSCs were seeded with defined volumes of αMEM, supplemented with 10% FCS and 1% P/S according to the fluid capacity of the scaffold (Chitosan film: 35 µL, Fibrin matrix: 25 µL, Collagen-GAG matrix: 40 µL and, Decellularized dermis:

22 µL). AdMSCs were suspended in αMEM and seeded dropwise directly onto the scaffold. After 1 h, 1 mL of additional medium was added to the scaffolds, which were further cultured under standard conditions.

3.2.3 Cellular distribution throughout scaffolds

AdMSC-containing scaffolds were rinsed with PBS, fixed (3.7% paraformaldehyde, 0.1% Triton in PBS) on ice for 30 min, and blocked in 2% BSA in PBS at 4°C overnight (n = 3, N = 3). Scaffolds were then incubated in a blocking solution containing 2 U/mL Texas Red-X Phalloidin (Life Technologies, Grand Island, NY) to stain polymerized actin and 3.5 µM To-Pro®-3 (Life Technologies) to stain DNA. After washing 4 times with PBS (10 min each), scaffolds were dried with sterile gauze, mounted in Vectashield® Mounting Medium (Vector Labs, Burlingame, CA) on glass bottom culture dishes (MatTek Corp., Ashland, MA), and imaged using an Olympus Fluoview FV10i confocal microscope (Olympus, Tokyo, Japan). Chitosan films were z-section imaged from top to bottom with the drop side facing down on the glass bottom, in 4 independent locations (one center and 3 periphery locations). As the fibrin matrix, collagen-GAG matrix, and decellularized dermis are too thick to image through from top to bottom, they were sectioned using a razor blade and rotated onto their sides in order to generate z-section images from cross-sections. Image analysis to assess cell morphology, number, and distribution was performed using Olympus FV10-ASW software (Olympus). Experiment performed by Thomas Peavy.

3.3 Scaffold *In Vitro* Assays

3.3.1 Metabolic activity and cytotoxicity in the scaffold

On days 1, 3, 7, and 14 after seeding, the metabolic activity and proliferation of the seeded cells was evaluated by precipitation of tetrazolium salt (WST-1). Cell death was measured by the release of lactate dehydrogenase (LDH) from the cells on days 1, 3, and 7 (both kits from Roche, Mannheim, Germany) (n = 3, N = 3). As the medium needed to be changed after 7 d, the total LDH activity could not be measured over a 14 d period. Seeded scaffolds were incubated in αMEM and WST-1 solution (1:10 ratio) for 1 h. The absorbance of the resulting formazan dye was measured at 450 nm with a reference wavelength of 620 nm. For the measurement of LDH activity, supernatants were harvested

from the same scaffolds used for WST-1 assay and the analysis was performed according to the manufacturer's instructions with the absorbance measured at 490 nm and a reference wavelength of 620 nm.

3.3.2 Characterization of secretion profile

Supernatants were collected from AdMSC seeded scaffolds or tissue culture plastic (n = 3, N = 3; 1.8 × 10^5 cells / scaffold) after 48 h under standard cell culture conditions, snap frozen with liquid nitrogen, and stored at -80°C until analysis. Human Cytokine and Angiogenesis Array Kits (R&D Systems, Abingdon OX, UK) were used to characterize the release of multiple cytokines and angiogenesis related proteins, respectively. Membranes were imaged using a Peqlab Fusion FX7 chemiluminescence system (Erlangen, Germany) and the spot intensity was quantified with ImageJ software (Schneider et al., 2012) using the MicroArray Profile plugin (OptiNav, Inc.). Scaffolds without cells served as controls.

3.4 *In Vivo* Chicken Chorioallantoic Membrane Assay

Research grade fertilized eggs (SPF, Valo Biomedia GmbH, Osterholz-Scharmbeck, Germany) were placed on a rotating egg tray for 3 days after fertilization at 37°C and 60-70% humidity. On day 3, a small window was made in the shell under aseptic conditions and the contents of the egg were gently placed into a 200 mL plastic dish. The dish was further placed into a petri dish with 50 ml of distilled water, 1% P/S, and 1% partricin and incubated at 70-80% humidity to prevent drying of the membrane. On day 10, autoclaved filter paper punches (5 mm) were added to the CAM directly followed by 10 µl of conditioned media collected from serum-free cell seeded scaffolds after 48 h in culture, αMEM, PBS, or 20 ng of VEGF, which was reapplied daily for 3 days (Dohle et al., 2009). The applied filter paper punches were imaged daily using a Canon EOS 20D digital SLR camera with a Canon EF 50mm f/1.8 II Standard AutoFocus Lens. Samples were quantified (n = 3, N = 6) by being given arbitrary values based on the distribution and density of CAM vessels around the filter paper punch as previously described (Ribatti et al., 2006) (Fig. 5).

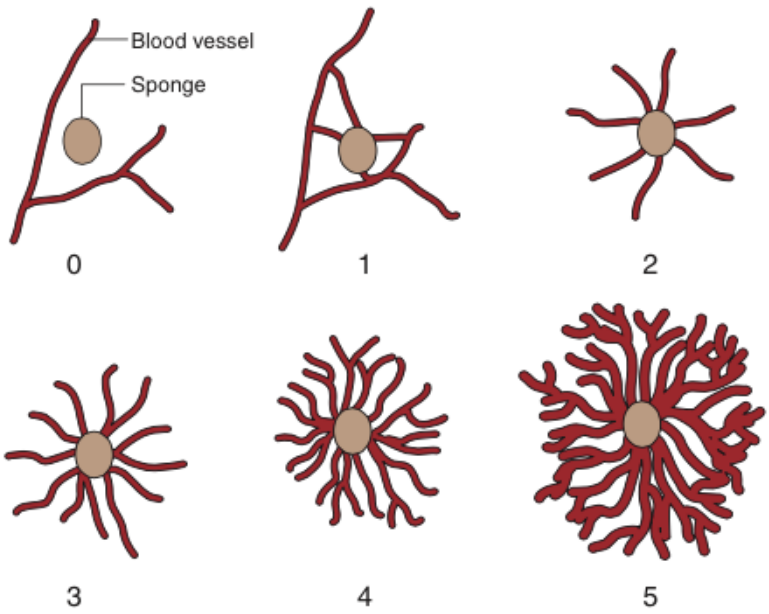

Figure 5. Scoring for angiogenic response by macroscopic evaluation of blood vessels ranging from 0-5. Graphic adapted from (Ribatti et al., 2006).

3.5 Hypoxia *In Vitro* Assays

3.5.1 Cell seeding and concentration

To determine the optimal seeding density for the collagen-GAG scaffolds (10 mm discs), AdMSCs were seeded in concentrations of 5×10^3, 5×10^4, 5×10^5, and 1×10^6 for comparison in a dropwise manner and allowed to adhere for 3 h in standard cell culture conditions. After this time, 1 ml of αMEM (Biochrom) supplemented with 10% Human Serum (Sigma) and 1% ab/am solution was added.

The metabolic activity of the AdMSCs on the scaffolds was examined using an alamarBlue® fluorometric assay (AbD Serotec, Raleigh, NC, USA) with a 4 h incubation time after 1, 7, and 14 d following manufacture's instructions (n = 3, N = 3). Scaffolds were then rinsed with sterile PBS and collected in 1x passive lysis buffer (PLB; Promega, Madison, WI), chilled for 10 min at 4°C, and pulse sonicated (SONICS Vibracell VCX130 Ultrasonic Cell Disrupter, USA) 10 times at 40% power to lyse the cells. To determine the amount of cellular proliferation, double stranded DNA was quantified using a PicoGreen assay kit (Invitrogen, Carlsbad, CA, USA) using the cell lysates (n = 3, N = 3).

3.5.2 Hypoxia and hypoxia-mimetic induction

After cells were seeded onto the collagen-GAG and allowed to adhere for 3 h, they were placed into a hypoxic incubator with 1% O_2 or deferoxamine mesylate (DFO; Sigma-Aldrich) was added to final concentrations of 30, 60, or 120 μM and incubated under standard cell culture conditions. Scaffolds seeded with AdMSCs cultured under standard conditions were used as a control.

3.5.3 HIF-1α quantification

To determine the HIF-1α concentrations, scaffolds were collected after 12 and 24 h, rinsed twice with sterile PBS, snap frozen with liquid nitrogen, and stored at -80°C until analysis. The total HIF-1α concentration was evaluated using an ELISA kit (Human/Mouse Total HIF-1α; R&D Systems, Minneapolis, MN, USA) according to manufacturer's instructions (n = 3, N = 3).

3.5.4 VEGF and SDF-1α release in vitro

To determine the release of VEGF and SDF-1α, the medium was removed from the scaffolds after 1, 3, and 7 d, snap frozen with liquid nitrogen, and stored at -80°C until analysis. The total concentrations were determined using a Human VEGF Quantikine ELISA kit and Human CXCL12/SDF-1 alpha Quantikine ELISA kit (R&D Systems), respectively, according to manufacturer's instructions (n = 3, N = 3). Due to high concentration levels, only 5 μl of the conditioned medium was used in the VEGF analysis.

3.6 *In Vivo* Mouse Wound Healing Model

Male hairless immunocompetent SKH1-Elite mice (Charles River; Germany) were used with four mice per group. Mice were allowed to adjust to the facility for 1 w prior to the operation. Each scaffold treatment was maintained in their respective cell culture conditions for 24 h prior to surgery. The groups consisted of control mice with scaffolds incubated in medium; scaffolds incubated in 120 μM DFO and AdMSC seeded scaffolds in normoxic conditions, environmentally induced hypoxic conditions (1% O_2), and chemically induced hypoxic conditions (120 μM DFO). Animals were fully anesthetized by inhalation of isofluorane (CP Pharmaceuticals Ltd., Wrexham, UK) and 0.07 ml of

buprenorphine was administered subcutaneously before wounding. Animals were kept warm by a heating pad and their eyes were dabbed with a lubricating ointment for the duration of the surgery.

Wounding was done with an 8 mm skin biopsy punch (Acuderm, Fort Lauderdale, FL, USA) on the left and right side of the back. TiMesh® extra light tetanized mesh (Nürnberg, Germany) was placed in the wound to avoid wound contracture and the scaffold was sutured (Ethilon nylon monofilament sutures 5-0; Ethicon, Norderstedt, Germany) into place. A V.A.C.® Therapy Dressing (KCI Medical Products, Wimborne Dorset, UK) was sutured in place over the wounded areas. Medical tape (Hansaplast, Hamburg, Germany) was further wrapped around the torso of the mouse to protect the wounded area and 0.03 ml of diazepam was administered subcutaneously before allowing the animal to recover near a heat lamp (Fig. 6). Animals were checked daily for well-being and given a 0.07 ml injection of buprenorphine daily as well as 0.03 ml of diazepam every three days.

After 14 d, the animals were euthanized with an overdose of isofluorane. The chest cavity was opened, blood was extracted from the heart, and the samples were placed on ice for 30 min. Samples were then centrifuged at 5,000 × g for 10 min. The serum was moved to a new tube and stored at -80°C until analysis. All bandages and sutures were removed and the animal was imaged. Then the skin of the back was cut away and the scaffolds were imaged with a transilluminator connected to a stereoscope optical microscope (Zeiss). The scaffolds were cut from the skin and half was stored in 3.7% formaldehyde for sectioning while the other half was snap frozen in liquid nitrogen and stored at -80°C until further analysis.

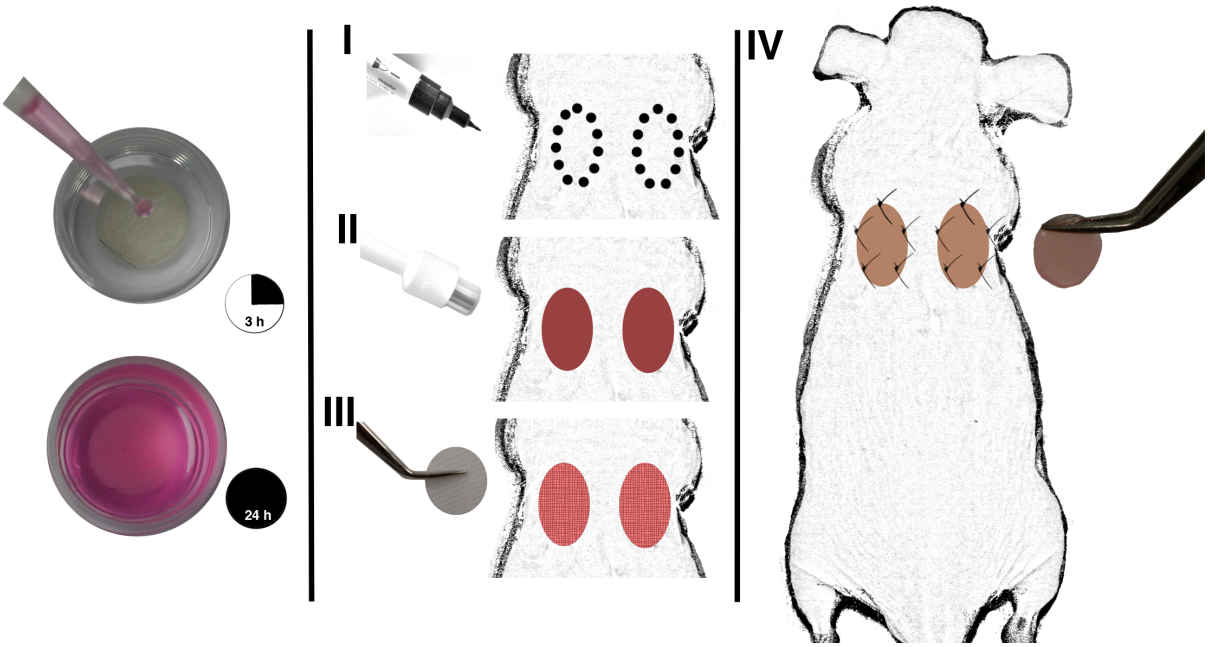

Figure 6. Bilateral full skin dermal regeneration model AdMSCs (50 µl) were seeded onto a 10 mm collagen-GAG substrate in a dropwise manner and allowed to adhere for 3 h. Medium was added (1 ml) and the substrate was exposed to either environmental or chemical hypoxia for a duration of 24 h. In the meantime, the mouse is prepared by marking a 8 mm circle on their back (I), the skin is removed with a biopsy punch (II), a titanium mesh is placed in the wounded area (III), and the collagen-GAG substrate is placed on top of the mesh and sutured in place (IV). A dermal bandage is sutured in place over the wounded area and the mouse's torso is wrapped further with medical tape (not pictured).

3.6.1 Digital segmentation

The vascular density of the harvested scaffolds was segmented from images obtained by transillumination using Vessel Segmentation and Analysis (VesSeg) software v0.1.4 (http://www.isip.uni-luebeck.de/index.php?id=150) (Egaña et al., 2009) (n = 2, N = 4). Images were converted to gray scale and via a semi-automated process a threshold was set to enhance vessel visualization. The images were further segmented so every white pixel was assigned to vessel-like structures and the rest was assigned as background in black. Further caution was taken in order to eliminate false-positive and false-negative structures.

3.6.2 Inflammatory protein levels

Serum collected from the mouse heart after 14 d was used to determine if there was an inflammatory response to the treatments (N = 4). A BD Cytometric Bead Array (CBA) Mouse Inflammation Kit (BD Biosciences; San Jose, CA, USA) was utilized in order to simultaneously measure levels of

Interleukin-6 (IL-6), Interleukin-10 (IL-10), Monocyte Chemoattractant Protein-1 (MCP-1), Interferon-γ (IFN-γ), Tumor Necrosis Factor (TNF), and Interleukin-12p70 (IL-12p70) with a BD FACSCanto™ II flow cytometer (BD Biosciences). Data was analyzed using FCAP Array™ Software v3.0 (BD Biosciences).

3.6.3 VEGF and SDF-1α release in vivo

To determine if the AdMSCs were still present and releasing growth factors, human VEGF and SDF-1α protein concentrations were measured from scaffolds collected from mice 14 d after surgery (n = 2, N = 4). The cells in the scaffolds were lysed with 300 µl lysis buffer (R&D Systems recipe for Lysis Buffer #11: 50 mM Tris (pH 7.4), 300 mM NaCl, 10% (w/v) glycerol, 3 mM EDTA, 1 mM $MgCl_2$, 20 mM β-glycerophospate, 25 mM NaF, 1% Triton X-100, 25 µg/ml Leupeptin, 25 µg/ml Pepstatin, and 3 µg/ml Aprotinin), pressed with a pestle, vortexed shortly, and left for 10 min on ice. Then the scaffolds were pressed once more with a pestle, shortly vortexed, and centrifuged for 5 min at 3000 × g at 4°C. The resulting supernatant was analyzed with a VEGF and SDF-1α ELISA (R&D Systems) where the VEGF was diluted 1:20, as with the *in vitro* analysis.

3.7 Statistical Analysis

Results were analyzed with GraphPad Prism® version 6.0e for Mac OSX (GraphPad Software, San Diego, CA USA) and are shown as mean ± standard deviation. Significant differences between sample groups were determined by analysis of variance (ANOVA) with a Bonferroni post-test where $p < 0.05$ was considered statistically significant. Asterisk denoting statistical significance are signified by: *$p < 0.05$, **$p < 0.01$, ***$p < 0.001$, and ****$p < 0.0001$.

4. RESULTS

4.1 Characterization of isolated adipose derived mesenchymal stem cells and dermal scaffolds

4.1.1 Characterization of isolated adipose derived mesenchymal stem cells

Adipose derived mesenchymal stem cells (AdMSCs) were isolated from human adipose tissue and characterized in terms of their differentiation potential and immunophenotype. As expected, the isolated AdMSCs showed a strong differentiation potential towards osteoblasts, adipocytes, and chondrocytes (Fig. 7). Calcium deposits were stained with Alizarin Red S for AdMSCs exposed to osteoblast differentiation medium. Lipid vacuoles from adipogenic differentiation were stained with Oil Red O. Chondrogenic pellets were stained with Alcian Blue to show chondrocyte growth.

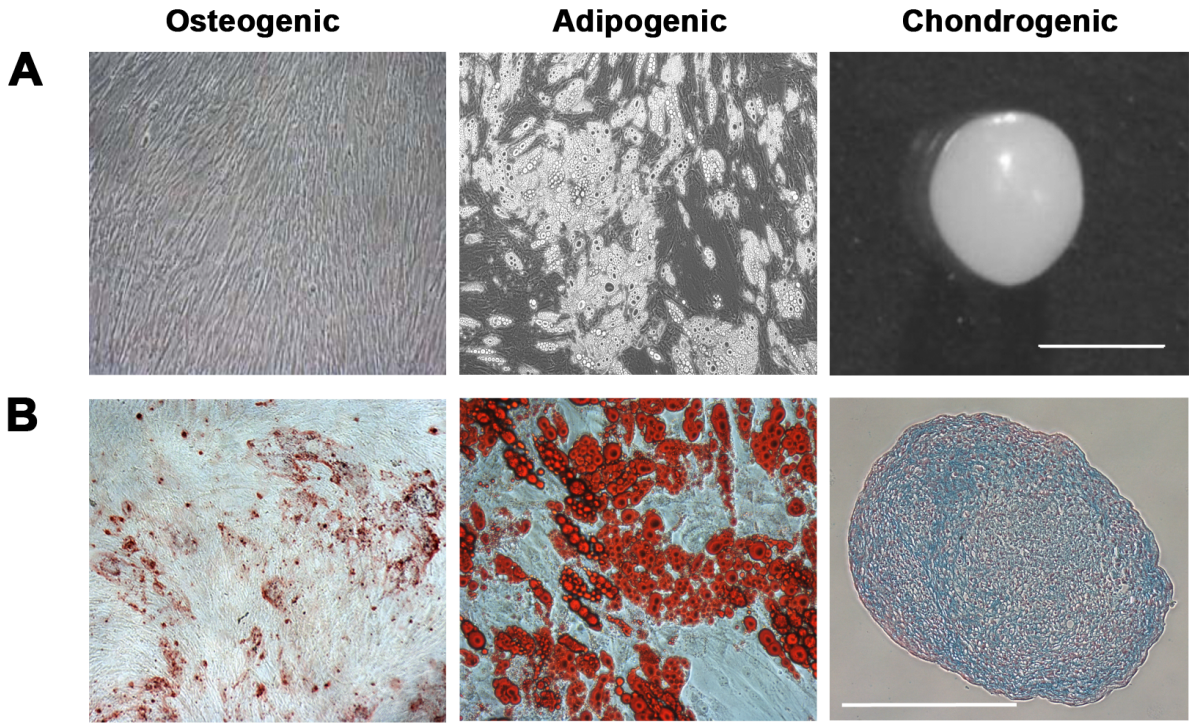

Figure 7. Differentiation of AdMSCs AdMSCs were seeded on tissue cultue plastic or in a pellet culture and differentiated with osteogenic, adipogenic, and chondrogenic supplemented medium (A). Stainings were performed after 21 days in culture. Alizarin Red S staining shows calcium deposits. (B left). Oil Red O stains lipid vacuoles red (B middle). Alcian blue reveals acetic mucins and acidic mucosubstances while a Nuclear Fast Red crossstain shows the nuclei (B right). Osteogenic and adipogenic images are represented at 10x magnification. Scale bar represents 1 mm. n = 3, N = 3

AdMSCs were further characterized in terms of their immune phenotypes and differentiation potential. Fluorescence-activated cell sorting (FACS) analysis showed that AdMSCs do not express the pan-hematopoietic marker CD45, but are positive for the mesenchymal markers CD73, CD90, and CD105 (Fig. 8). Interestingly, AdMSCs expressed very low levels of the pericyte marker CD146

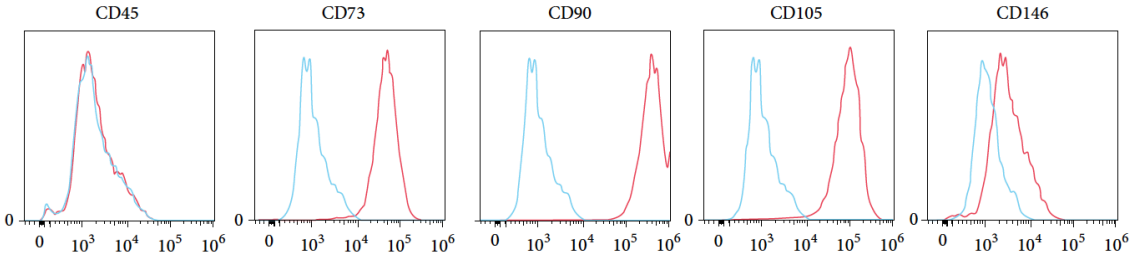

Figure 8. Fluorescence-activated cell sorting characterization of AdMSCs The immune phenotype of the cells was evaluated by labeling cells with Phycoerythrin-conjugated antibodies for flow cytometry. The blue histogram indicates the isotype control. n = 3, N = 3

4.1.2 Scaffold characterization

Scaffolds should be biocompatible to their desired application and consist of a porous network to facilitate cell migration and communication. In this work, four different scaffolds were compared for their usability in dermal regeneration (Table 1). First, the macro- and microstructure of the four scaffolds was evaluated and compared, observing important differences (Fig 9). The dry thickness of the scaffold varies from a minimum of 0.22 mm for chitosan films to 3.8 mm for fibrin matrices (Fig 9A). When wet, the structure of fibrin matrices collapsed to a fibrous mesh decreasing the measurable thickness. The decellularized dermis had the thickest structure at 1.5 mm, while the collagen-GAG matrix was 0.22 mm thick (Table 1). Compared to the other scaffolds, chitosan has a film-like appearance, while the fibrin and collagen-GAG present a more mesh-like structure and exhibited high porosity throughout the scaffold. The decellularized dermis exhibited much tighter pores and the chitosan did not have any visible porosity (Fig. 9B).

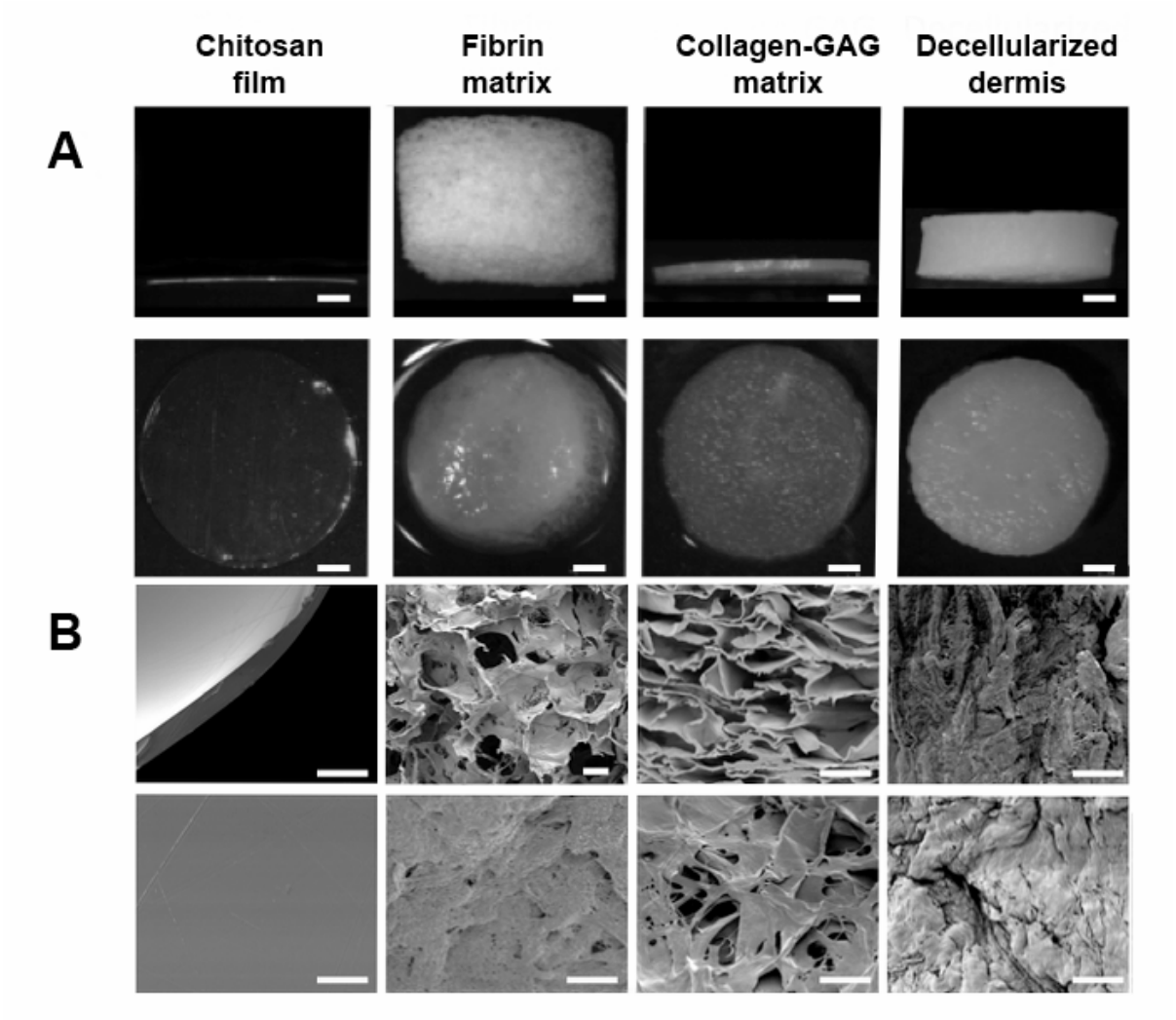

Figure 9. Characterization of the scaffolds Scaffolds (6 mm in diameter) were macroscopically imaged from the side (dry, top row) and the top (wet, bottom row) using a stereoscopic microscope. While the other scaffolds maintain their structure when wet, the fibrin matrix collapses into a mesh of fibers (A). Scale bars represent 1 mm. The pore structure and texture of the scaffolds as analyzed by SEM micrographs from the transverse sections (top) and top view (bottom) (B). Note the complete absence of pores in the chitosan film in comparison to the fibrin matrix, collagen-GAG matrix, and the decellularized dermis. Scale bars represent 100 μm. (SEM micrographs taken by Ursula Hopfner.) n = 3

Table 1. Comparison of scaffold properties The general properties of the scaffolds show a broad variation in weight, size, fluid capacity, and price of material. As the fibrin matrix is currently not commercially available some information could not be divulged.

	Commercial Name	Company	Price [USD/cm²]	FDA approval	Dry Weight [mg/cm²]	Fluid capacity [µl/cm²]	Dry thickness (mm)
Chitosan film	**BioPiel®**	Recalcine	10	Yes	4 ± 0.3	123 ± 14.8	0.12
Fibrin matrix	**Smart Matrix™**	RAFT	-	N/A	12 ± 1.5	87 ± 9.0	3.8 – 1.8
Collagen-GAG matrix	**Integra® DRT**	Integra Life Sciences	3	Yes	10 ± 1.4	143 ± 5.6	0.22
Decellularized dermis	**Strattice™**	LifeCell	26	Yes	148 ± 2.9	77 ± 4.1	1.5

4.2 Adipose-derived mesenchymal stem cells seeded on four different scaffolds

4.2.1 Cellular attachment and distribution

Differences in the mechanical properties should influence the cell behavior when seeded. For that, a detailed view into the interaction and distribution of the seeded cells in the four different scaffolds was obtained by confocal microscopy. Except for the decellularized dermis, the AdMSCs were highly attached to the material, showing fibroblastic morphology and strong intercellular interactions, creating a complex tridimensional arrangement between the cells and the scaffold (Fig. 10A). The images were analyzed to give quantitative, spatial information on the cellular distribution throughout the scaffold (Fig. 10B). The AdMSCs formed a layer on the seeding surface of chitosan films, showing almost no cells in the core. In the case of the fibrin matrix, cells were observed throughout the scaffold with a tendency to accumulate at the center of the material. Cells seeded on collagen-GAG matrices also showed a different distribution pattern creating a cell gradient from the seeding side to the bottom. In the decellularized dermis, AdMSCs were more concentrated on the seeding side while migration through the scaffold was limited.

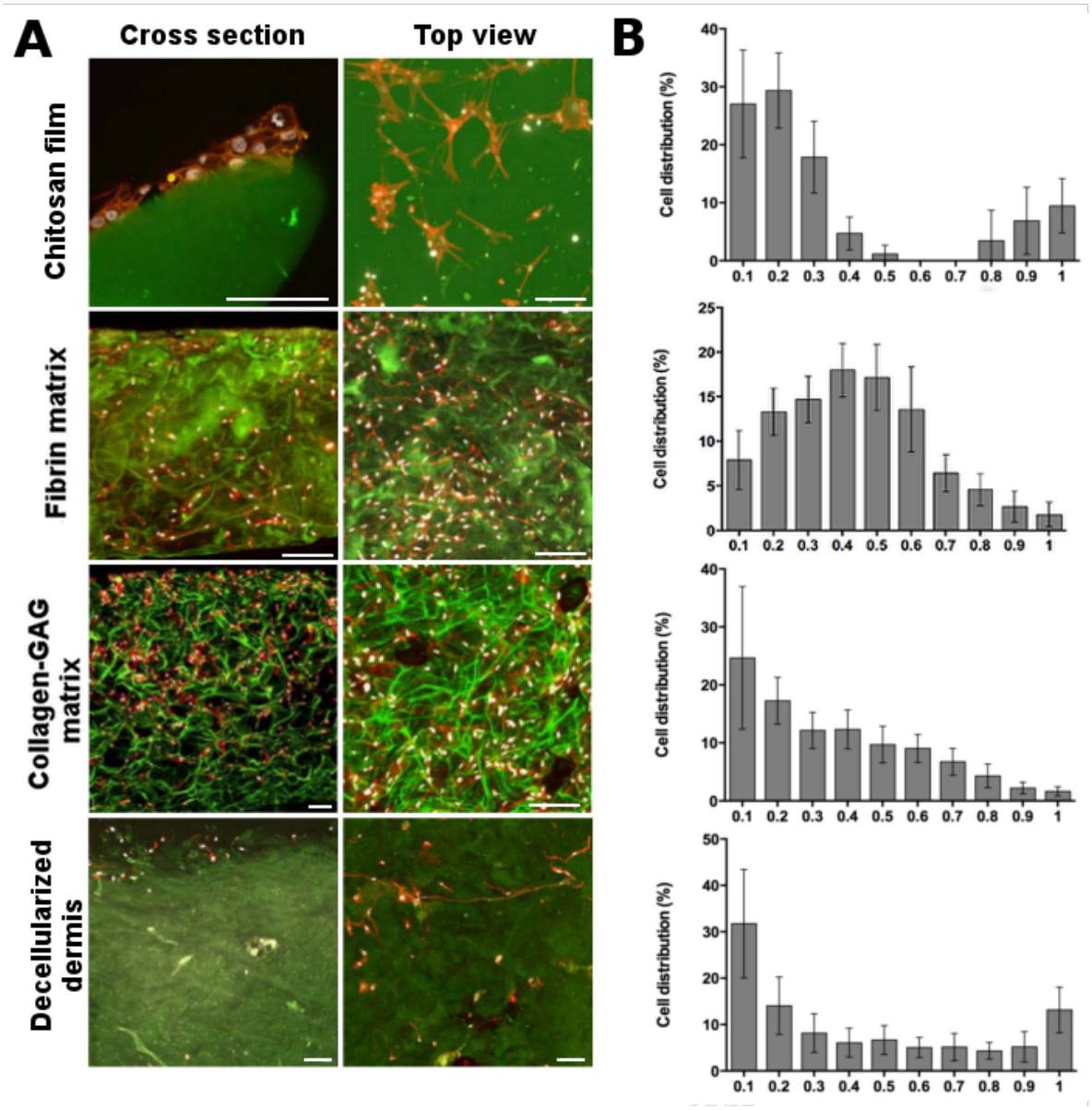

Figure 10. Cellular distribution and attachment of cells on scaffolds After seeding, the distribution and attachment of the cells was evaluated by LSM. In all cases, except for the decellularized dermis, cells (stained with To-Pro®-3 (white) / phalloidin (red)) adhered to the scaffold (green autofluorescence) showing a fibroblast like morphology. As can be seen in the first column, cells formed a layer over chitosan films while in the others cells were able to further migrate into the scaffold. Cross section (right) and top view (left) of scaffolds. Scale bar represents 150 µm (A). Quantification of the cellular densities after 1 day throughout sections, ranging from the top (0.1) to the bottom (1) of the scaffolds as seen in confocal imaging (B). n = 3, N = 3 (Images and quantification by Dr. Thomas Peavy.)

4.2.2 AdMSC biocompatibility with scaffolds

The distribution of AdMSCs is clearly an important indicator for the biocompatibility with the different scaffolds. However, the secretion activity relies on cell survival beyond the initial seeding, which was

measured indirectly by means of their metabolic activity. Twenty-four hours after seeding, the formation of formazan blue, as an indicator of metabolic activity, was highest in fibrin and collagen-GAG matrices, while AdMSCs seeded on chitosan film and decellularized dermis initially showed comparable values (Fig. 11A). In order to evaluate if these differences were due to increases in cellular death, Lactate dehydrogenase (LDH) activity was measured from the supernatants. LDH is released from the cell only after loss of membrane integrity as in the case of cell death. It can be seen that the decellularized dermis had a high rate of cytotoxicity (almost 100%), even after only one day in culture, whereas the collagen-GAG matrix had virtually no cytotoxic effect (Fig. 11B).

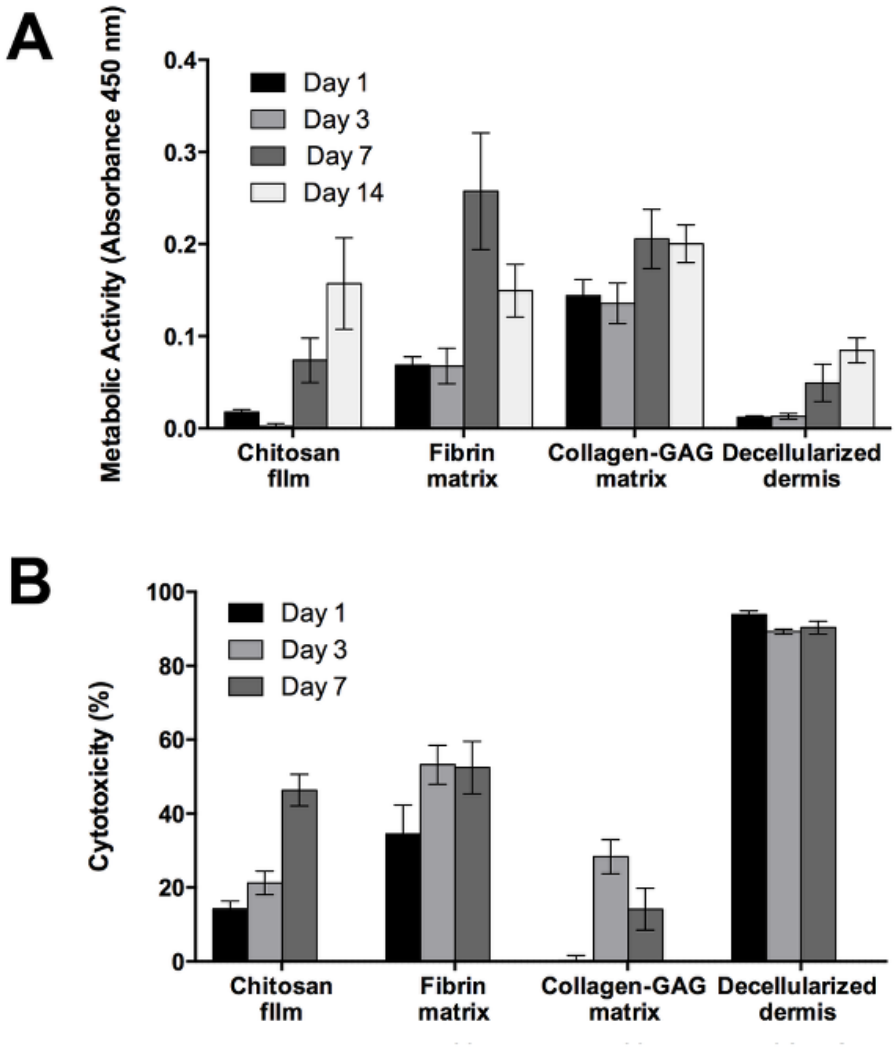

Figure 11. Cellular survival within the scaffolds The metabolic activity (WST-1) and cellular death (LDH) was measured and compared after seeding. Results show that the metabolic activity of the cells increased over time, indicating that the cells were able to proliferate within the scaffolds (A). The LDH released by the cells was measured as an indicator of cellular death. The highest mortality was observed after only 1 d in the decellularized dermis indicating a poor biocompatibility with the AdMSCs (B). n = 3, N = 3

The long-term viability of the AdMSCs seeded on the scaffolds was measured and compared at further time points after seeding. Our results show that, while the chitosan film and decellularized dermis had comparable metabolic activity through day 7, 14 days after seeding the chitosan film had comparable results to the fibrin and collagen-GAG matrices (Fig. 11A). The collagen-GAG matrix showed steady metabolic activity throughout the 14 days, while the fibrin matrix showed an increase in activity through day 7 after which the activity decreased at day 14. Cellular death results showed a general increase in cytotoxicity as the metabolic activity of the cells increased, except for day 7 of the fibrin and collagen-GAG matrix where the metabolic activity was higher than the rate of cell death. The highest percentage of cytotoxicity was seen in the decellularized dermis being close to 100% (Fig. 11B).

4.3 Growth factor and cytokine release from cell seeded scaffolds

4.3.1 Secretion profile

The differences in biocompatibility lead to the conclusion that depending on the physical and chemical conditions AdMSCs are exposed to within a given scaffold the secretion profile could vary considerably. Here, the secretion of 91 different angiogenic, cytokine, and chemokine factors were analyzed to obtain a characteristic secretion profile for each scaffold. Among the detected factors, the most prevalent ones were macrophage migration inhibitory factor (MIF), plasminogen activator inhibitor 1 (Serpin E1), interleukin 6 (IL-6), interleukin 8 (IL-8), chemokine (C-X-C motif) ligand 1 (CXCL1), placental growth factor (PlGF), and vascular endothelial growth factor (VEGF) (Fig. 12). Due to the low viability of the cells observed after seeding, decellularized dermis scaffolds were excluded for this assay.

Compared to AdMSCs seeded directly onto tissue culture plastic, the scaffold condition itself significantly induced the release of PlGF while it reduced the release of VEGF ($p < 0.05$). Compared among the scaffolds, we observed that the release of angiogenesis inducing IL-8 was similar between fibrin matrices and two-dimensional cultures, while chitosan films and collagen-GAG show a dramatic decrease ($p < 0.05$). The release of inflammation regulating IL-6 was elevated in supernatants from

cells seeded on collagen-GAG matrices while chitosan films showed the highest expression of Serpin E1. MIF and CXCL1 did not show any significant differences between scaffolds or control conditions.

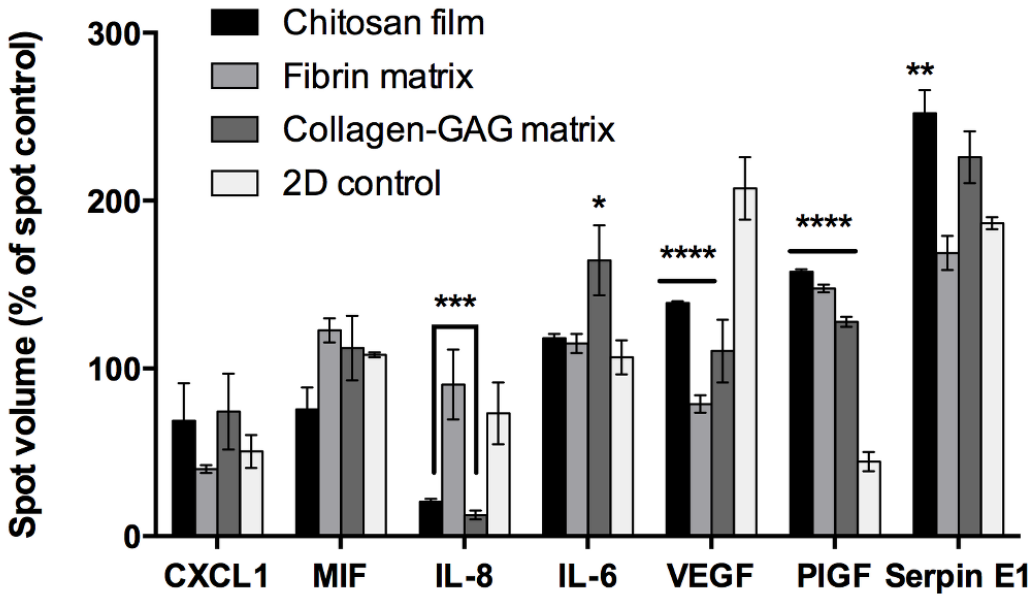

Figure 12. Secretion profile of AdMSC seeded scaffolds Human cytokine and angiogenesis arrays were utilized in order to analyze supernatants after 48 h incubation to detect if there is an effect of the scaffolds interaction with the cells on paracrine factor release. Decellularized dermis scaffolds were excluded as previous data revealed that it did not provide a compatible environment for the cells to migrate and flourish. Chitosan films and collagen-GAG matrices show a decrease in expression of IL-8 in comparison to fibrin matrices, which is similar to two-dimensional conditions. Collagen-GAG matrices had a significant release of IL-6, while chitosan films had an increase of Serpin E1 release over all other conditions. There are significant differences in release of PIGF and VEGF from all scaffolds in comparison to two-dimensional cultures. *$p < 0.05$; **$p < 0.01$; ***$p < 0.001$; ****$p < 0.0001$ when compared to 2D control. n = 3, N = 3

4.3.2 Effect of secreted factors from AdMSC seeded scaffolds to induce angiogenesis in vivo

Finally, we evaluated the biological effects of conditioned medium in an *in vivo* CAM assay model. Based on the different release profiles obtained *in vitro*, it can be assumed that the angiogenic response *in vivo* is visible. The chicken chorioallantoic membrane assay is an established method to monitor *de novo* vessel formation. Here, conditioned medium was pipetted onto autoclaved filter paper punches in order to determine if there was an enhanced effect of the factors secreted from the AdMSC that was due to the composition of the scaffold or if the scaffold alone had any angiogenic potential. In order to minimize irritation to the CAM, the scaffolds themselves were not utilized. In the

positive control (VEGF), large existing vessels showed a tendency to move towards the filter paper, while this was not evident in the samples exposed to AdMSC conditioned medium suggesting that overall the supernatant of AdMSC was not as pro-angiogenic as pure VEGF (Fig. 13A). Nevertheless, as seen in the *in vitro* data, the highest instance of neovascularization in small vessel convergence and growth occurred with medium that was obtained from collagen-GAG matrices followed by fibrin matrices and, finally, chitosan films. The quantification is based on arbitrary points given for *de novo* small vessel formation up to reorganization of existing vessels (Fig. 13B, also see Fig. 5 in methods and materials) (Ribatti et al., 2006). These results suggest that the composition of the scaffold has a direct effect on the angiogenic factors released from the AdMSCs. No significant differences appeared between PBS, conditioned medium without cells, and αMEM alone (data not shown for the medium exposed samples).

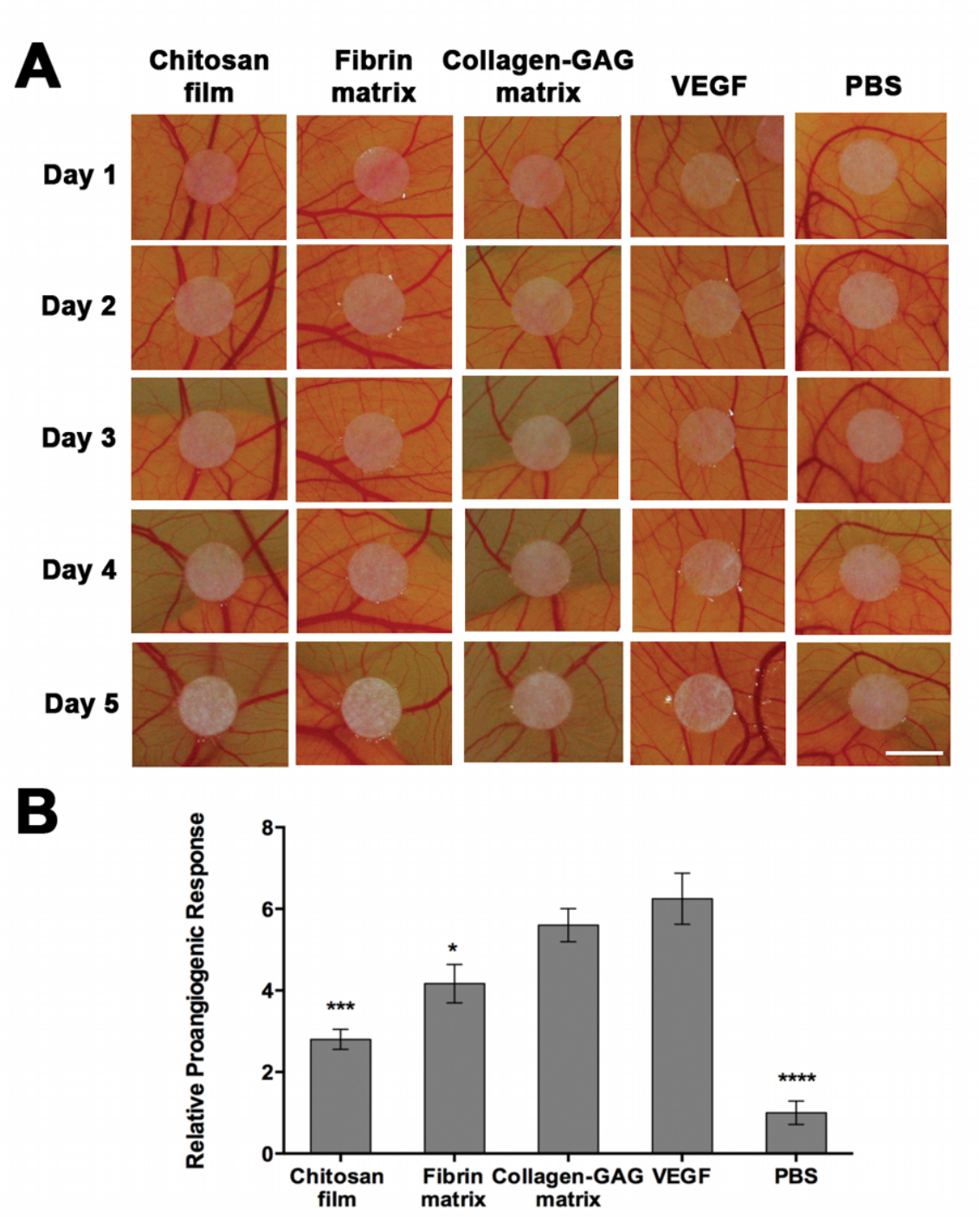

Figure 13. Chicken chorioallantoic membrane *in vivo* analysis Autoclaved filter paper punches with conditioned medium from scaffolds after 48 h in culture were observed over a five day period for neovascularization of the CAM. Note the increase in small vessel convergence from the scaffold, specifically in VEGF, collagen-GAG, and fibrin matrices. Samples exposed to conditioned medium without cells are not pictured, as they did not differ from the negative control (PBS) (A). Growth was analyzed from 6 replicates per treatment based on an arbitrary scoring system dealing with new small vessel formation and the behavior of existing vessels as observed daily according to [27]. Briefly, a value was assigned for each 5 d ranging from (0) unchanged, to slight changes in density and convergence towards filter paper punch (1), and further increases in density and convergence (up to 5) (B). Scale bar represents 5 mm. *$p < 0.05$, ***$p < 0.001$, ***$p < 0.0001$ when compared to VEGF positive control. n = 6, N = 6

4.4 Optimization of AdMSC seeded collagen-GAG in hypoxia and hypoxia-mimetic conditions to improve paracrine secretion of regenerative molecules

4.4.1 Cellular density

To determine the appropriate seeding density of AdMSCs on 10 mm discs of collagen-GAG matrices for optimal survival, proliferation, and stability over time, cells were seeded at different densities and evaluated (Fig 14). The metabolic activity per dsDNA was quantified over a period of two weeks. During this time 5×10^5 cells were determined to be the optimal seeding density for the size of the scaffold as the cells maintained stable activity over two weeks time. With 5×10^3 cells, the activity was too low to be desirable and 5×10^4 cells had good growth but the initial activity at day 1 was lower than desired (Fig. 14B). With 1×10^6 seeded cells, the cellular activity decreased at each time point indicating the cells may have been overcrowded.

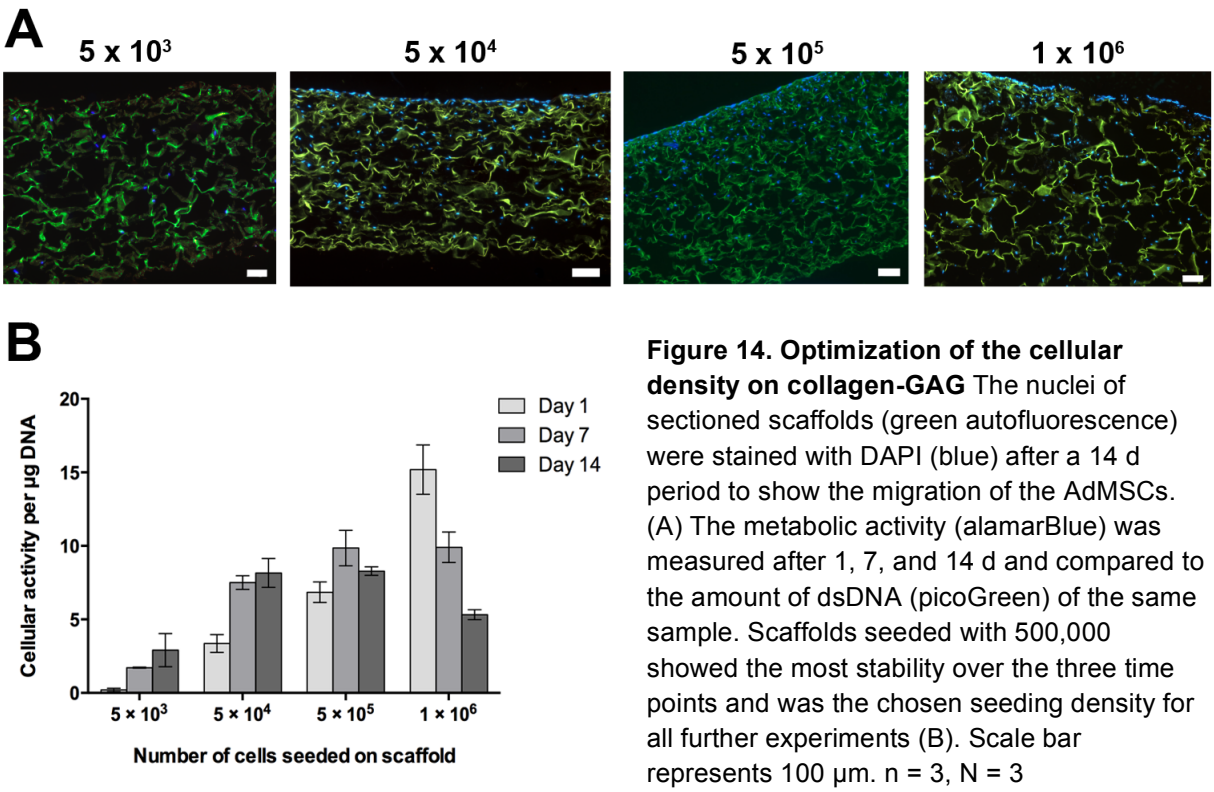

Figure 14. Optimization of the cellular density on collagen-GAG The nuclei of sectioned scaffolds (green autofluorescence) were stained with DAPI (blue) after a 14 d period to show the migration of the AdMSCs. (A) The metabolic activity (alamarBlue) was measured after 1, 7, and 14 d and compared to the amount of dsDNA (picoGreen) of the same sample. Scaffolds seeded with 500,000 showed the most stability over the three time points and was the chosen seeding density for all further experiments (B). Scale bar represents 100 µm. n = 3, N = 3

4.4.2 Effect of cellular preconditioning on hypoxia related proteins

As DFO creates a hypoxia-mimetic environment through the upregulation of HIF-1α, the total concentration from cell lysates was quantified after 12 and 24 h by ELISA in order to determine if there was a difference in release from environmentally and chemically induced hypoxia and, furthermore, if a concentration dependent release from the chemically induced hypoxia existed. AdMSC seeded scaffolds that were exposed to standard cell culture conditions were utilized as a control where no HIF-1α could be detected (data not included). No expression was detected from any sample after 24 h in culture. No significant differences could be detected between AdMSC seeded collagen-GAG that was exposed to 1% O_2, 30 μM DFO, or 60 μM DFO. The highest instance of HIF-1α was detected when AdMSCs were exposed to 120 μM DFO (Fig. 15).

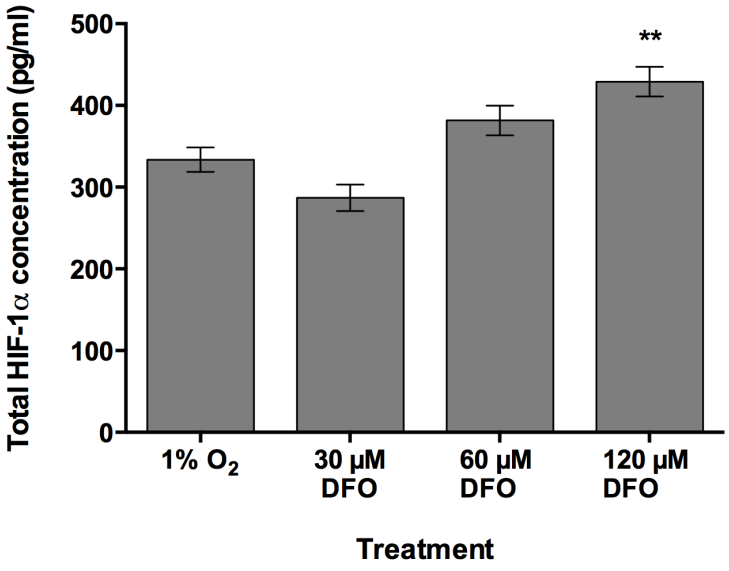

Figure 15. Total HIF-1α protein quantification from cell lysates *in vitro* The total HIF-1α concentration was quantified from cell lysates by ELISA after 12 h in culture. With increasing concentrations of hypoxia-inducing DFO, a higher HIF-1α concentration could be measured in the cell lysates. The release of HIF-1α under environmental hypoxia was equivalent to 30-60 μM of DFO. ***p* < 0.01 when compared to 1% O_2. n = 3, N = 3

To further determine the potential of the preconditioning, hypoxia and angiogenesis related paracrine factors, VEGF and SDF-1α, were quantified. No significant differences could be seen after one day between treatment groups in either protein concentration. After days 3 and 7, a significantly higher

amount of VEGF was secreted from cells exposed to 120 μM DFO than those under standard cell culture conditions (Fig. 16A). There was a significantly lower amount of SDF-1α released from cells under environmental hypoxia compared to other conditions after 7 days. DFO alone showed a strong release of SDF-1α after 7 days, which did not appear to be concentration dependent. Only after 3 days was there an increase of release from cells exposed to 120 μM DFO in comparison to lower concentrations (Fig 16B).

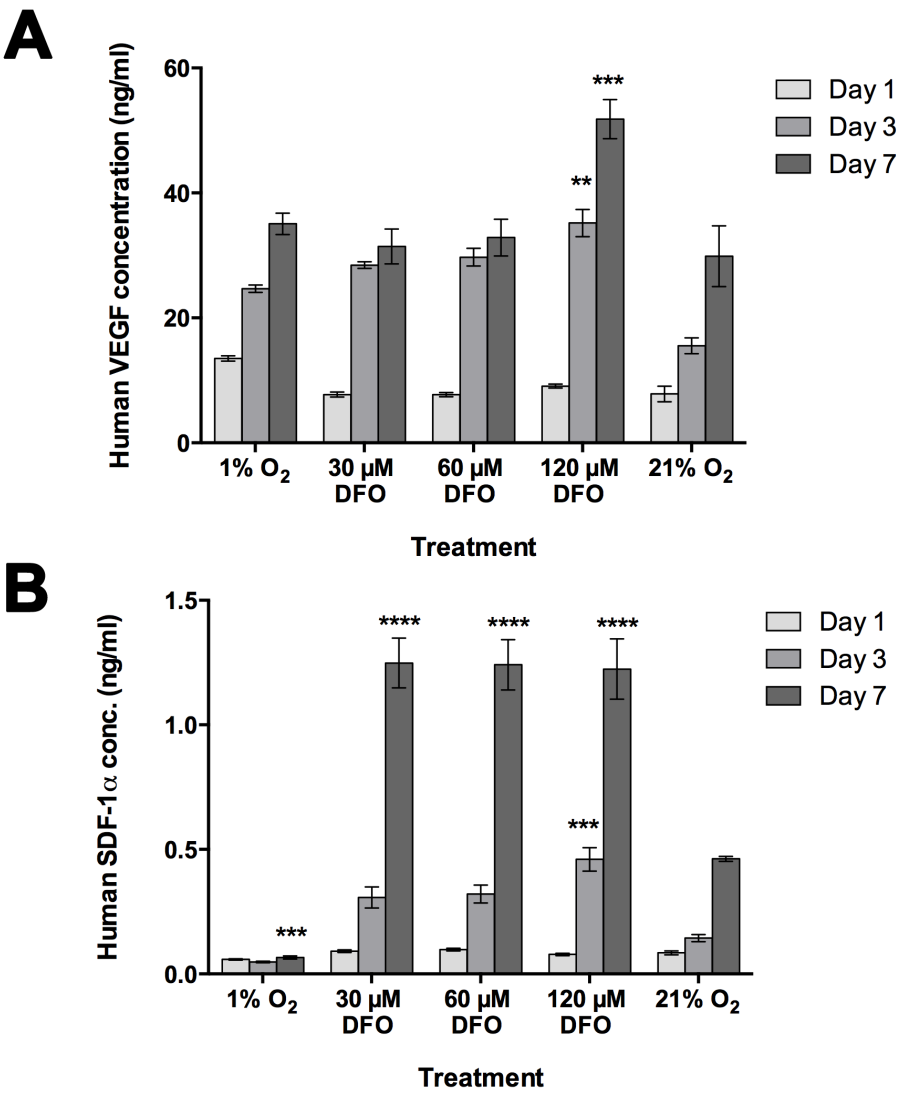

Figure 16. VEGF and SDF-1α release from collagen-GAG scaffolds *in vitro* VEGF and SDF-1α expression was quantified from cell culture supernatants by ELISA. The release of VEGF was seen in higher concentrations in AdMSCs exposed to 120 μM DFO after 3 and 7 d (A). Alternatively, a higher concentration of SDF-1α was released from cells when exposed to environmental hypoxia, although the concentration did not affect the release in a significant way (B). Significance is indicated by $^{**}p < 0.01$, $^{***}p < 0.001$, $^{****}p < 0.0001$ when compared with the 21% O_2 control samples. n = 3, N = 3

4.5 Evaluation of pro-angiogenic potential of preconditioned AdMSC collagen-GAG scaffolds *in vivo*

Due to the observed advantage of a higher DFO concentration, 120 μM was used for *in vivo* evaluation. Preconditioned AdMSCs seeded collagen-GAG matrices were transplanted in immunocompetent mice and allowed to remain for 14 days in order to detect neovascularization.

4.5.1 Inflammatory response of pre-conditioned cell seeded scaffolds

To determine if there was a systemic inflammatory response from the treatment in the mice, the serum was collected and six inflammatory markers were checked by FACS analysis (Fig. 17). IL-10 and IFN-γ did not show expression in any of the treatments while IL-12p70 and TNF did not show any significant differences between treatment groups. MCP-1 showed a higher concentration in mice exposed to DFO treated cells and expression of IL-6 show a highly significant ($p < 0.0001$) increase of expression in DFO exposed cells in comparison to those treated in environmental hypoxic or normoxic conditions.

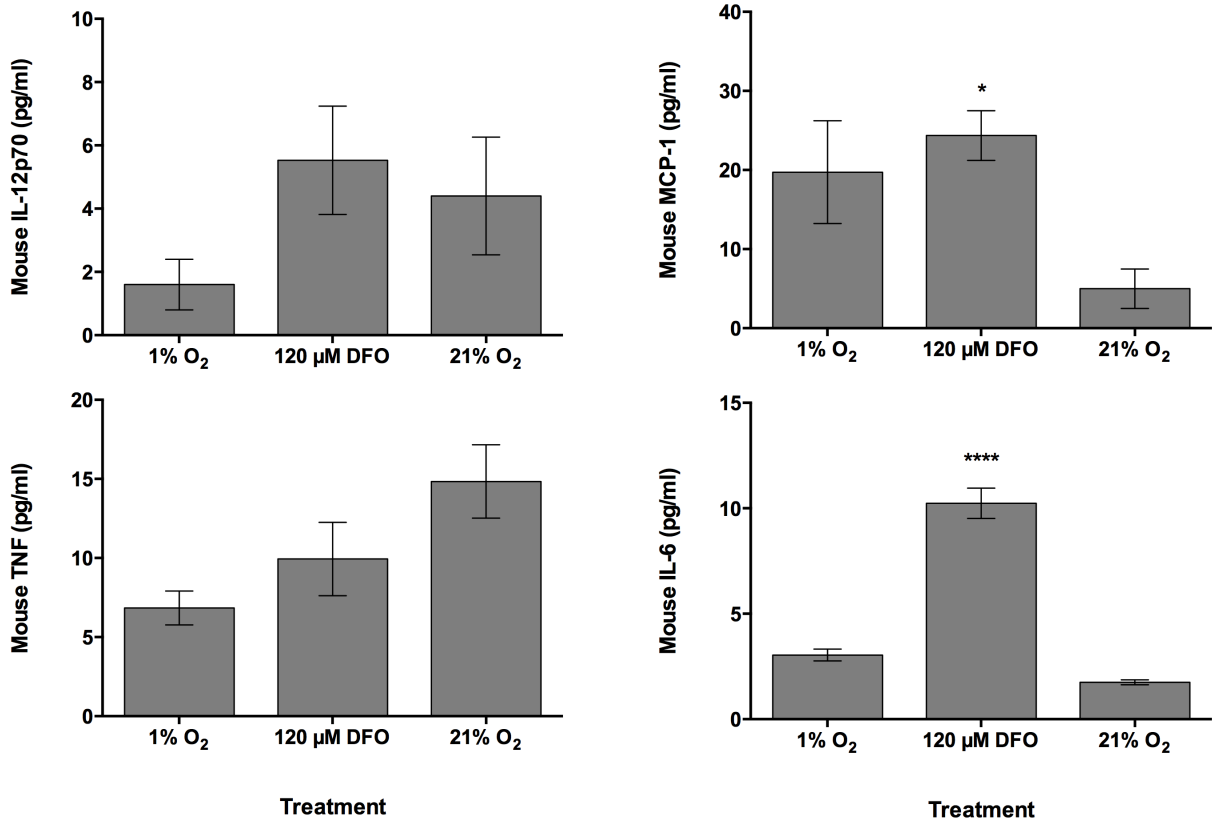

Figure 17. Inflammatory factor release *in vivo* A flow cytometer analysis was run using serum obtained from the mouse heart 14 d after surgery. Expression of IL-12p70 and TNF did not show any significant differences between treatments. While MCP-1 and IL-6 showed higher levels of occurrence in samples that were exposed to DFO. In addition, IL-10 and IFN-γ were analyzed but no expression was seen. Significance is indicated by $*p < 0.05$, $****p < 0.0001$ when compared to the 21% O_2 control. N = 4

4.5.2 Influence of pro-angiogenic potential of preconditioning on angiogenesis

Scaffolds were harvested from the mice and immediately imaged with a transilluminator to detect neovascularization (Fig. 18). The digital segmentation of the images revealed a higher density of vessel structures in scaffolds that had AdMSCs exposed to hypoxic conditions (Fig. 18B). Vessel growth can also be seen when there were no cells and with AdMSCs exposed to normoxic conditions but to a lesser extent.

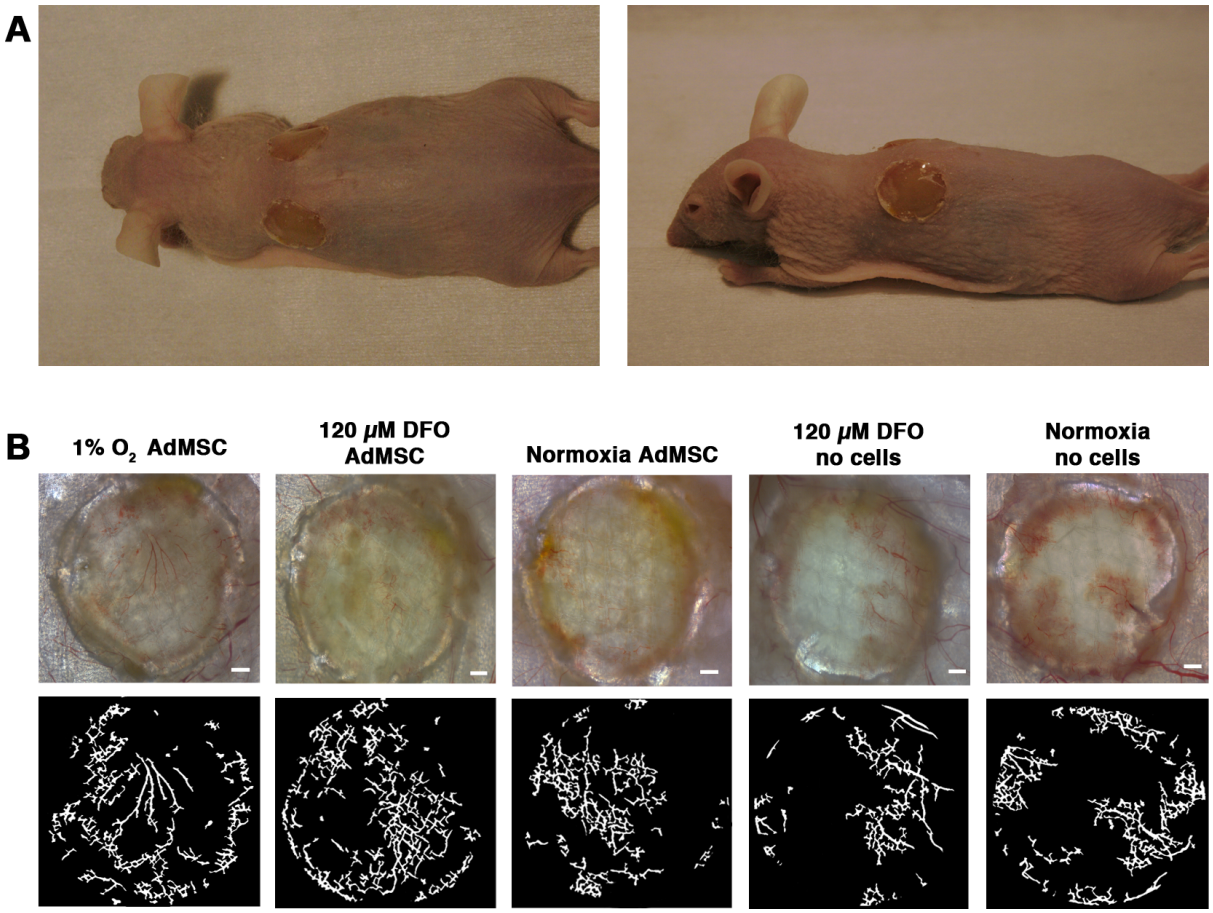

Figure 18. Vascularization of collagen-GAG scaffolds Nude immunocompetent male mice with a 10 mm collagen-GAG substrate 14 d after surgery (A). Neovascularization in the collagen-GAG substrate was analyzed by transillumination and digital segmentation using VesSeg software to highlight vessel structures (B). Pre-seeded scaffolds with AdMSCs showed the highest levels of de novo vessel formation when hypoxia was environmentally or chemically induced. Scale bar indicates 1 mm. n = 2, N = 4

4.5.3 Release of hypoxia related pro-angiogenic factors from in vivo

In order to determine if the AdMSCs remained on the scaffolds and were protected from immune detection by the mice, the harvested scaffolds were checked for the presence of human VEGF and SDF-1α. As with *in vitro* results, there was a higher instance of VEGF detected with cells exposed to 120 μM DFO than normoxic or environmentally hypoxic conditions (Fig. 19A). Although, differing from *in vitro* results, the levels of SDF-1α remained similar between AdMSC treated groups (Fig 19B). Those that did not have cells seeded on them did not show any expression of VEGF or SDF-1α, indicating that no factors of mouse origin were detected with the antibodies.

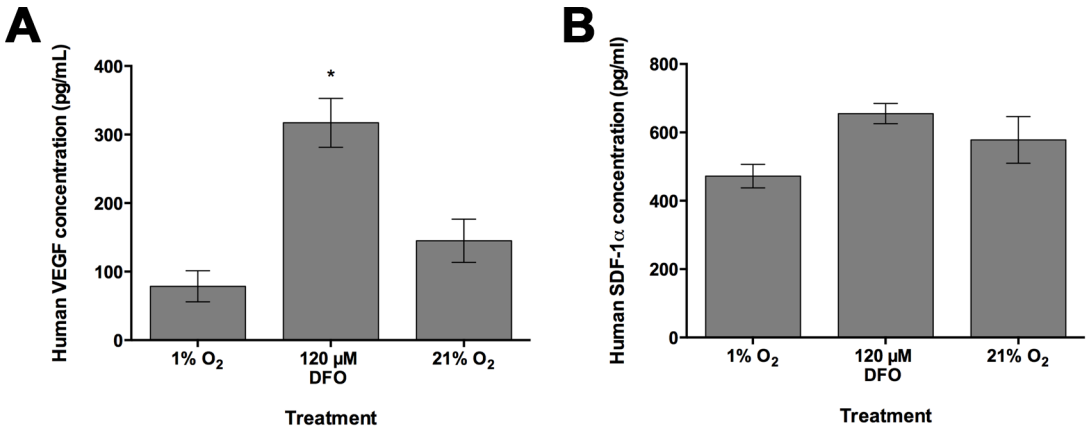

Figure 19. VEGF and SDF-1α release *in vivo* Collagen-GAG substrates harvested from mice after 14 d were evaluated for human VEGF (A) and SDF-1α (B) concentrations released from the AdMSCs, which were quantified from cell lysates by ELISA. Significantly high levels of VEGF expression were detected from samples exposed to DFO. Significance is indicated by $*p < 0.005$ when compared with the 21% O_2 control. n = 2, N = 4

5. DISCUSSION

5.1 Impact of scaffold characteristics on the potential for a synergistic regenerative response of AdMSCs

Although various stem cell populations have been described for therapeutic use, MSCs are particularly attractive as they are well discerned and ongoing clinical trials have shown promising results in wounded tissue (Dash et al., 2014; Jackson et al., 2012; Maxson et al., 2012; Shin and Peterson, 2013). Furthermore, there is great potential for the use of AdMSCs in regenerative medicine (Mizuno et al., 2012). They are easy to isolate, accessible with minimally invasive procedures, contain a high number of cells within only a small amount of tissue (Aust et al., 2004), and the age of the patient does not affect their proliferation rate or differentiation potential (Chen et al., 2012; Mirsaidi et al., 2012) making them ideal for clinical procedures.

For clinical application, the administration and effectiveness are key factors to describe the usability of a given treatment. In the case of AdMSCs, this encompasses the viability under the given conditions and their ability to release beneficial growth factors to the damaged tissue. Administration of the cells alone is problematic as the cells may migrate out of the wound bed and their effects can be lost. To minimize migration, dermal scaffolds have been used. Furthermore, these scaffolds have been shown to promote wound healing by releasing growth factors. The scaffolds examined in this work were of particular interest as they are currently used or being tested for use in clinics, although their healing effectiveness to date is subpar due to slow tissue revascularization. The viability, migration, and growth factor release, especially of the angiogenic growth factors, were of particular interest in this study.

AdMSCs and scaffolds were analyzed separately for individual characteristics. While there are no certain surface markers to identify AdMSCs some are known to occur regularly and can be identified through FACS analysis. As shown in Fig. 8, the cells used in this study were positive for CD73, CD90, CD105, and CD146 and lacked CD45. In addition, the cells were able to differentiate towards the osteogenic, adipogenic, and chondrogenic lineages. It can, therefore, be concluded that the extraction of the AdMSCs from donor tissue was successful. On the other hand, the four chosen scaffolds

differed substantially in their composition and properties (Table 1). Consequently, the distribution and attachment of the cells seeded into the different scaffolds were compared. AdMSCs were able to attach to all four types of scaffolds but due to their physical differences, the cellular distribution, viability, and proliferation greatly varied.

As the stiffness of a scaffold can determine the cell fate, it is important to take this into consideration when determining which material is used and what is the desired end goal. In the case of skin, a more flexible scaffold that mimics its natural environment would be the most suitable. In addition, the microenvironment or niche of the stem cells, the three-dimensional space, is critical for the cells to communicate and thrive (Mohyeldin et al., 2010). Therefore, the scaffolds need to create a welcoming environment for the cells as they are in their native conditions.

5.1.1 Scaffold structure and cellular interaction

5.1.1.1 Chitosan film

Consistent with the lack of porosity detected in chitosan films (Fig. 9), cells created a single layer on the seeding side, with virtually no penetration into the material (Fig. 10). Other chitosan-derived scaffolds contain artificial pores in order to facilitate cell migration (Ma et al., 2009; Tully-Dartez et al., 2010). The seeding side is critical for chitosan-based scaffolds to generate either a superficial cell layer or create an AdMSC interface between the scaffold and the wound bed. As there is only a layer of cells, these may migrate out soon after transplantation and the effects of the AdMSCs to the wound bed may be beneficial for a short time in order to start a pathway towards healing. While the metabolic activity increased over time, there may be an overcrowding of the cells that could limit the potential of the AdMSCs to release healing factors. The antimicrobial properties of chitosan does make it a beneficial treatment for superficial wounds and burns to minimize scaring, decrease pain sensation, and reduce inflammation (Dai et al., 2011).

5.1.1.2 Collagen-GAG and fibrin matrix

In contrast to the chitosan film, the AdMSCs seeded onto the fibrin and collagen-GAG matrices showed better penetration into the material (Fig. 10). The cellular distribution in fibrin matrices peaked

at the center of the scaffold. This effect may be due to the porosity at the center of the fibrin matrix appearing to be uneven, showing a larger pore structure on the top and bottom of the scaffold as compared to the center, which could inhibit the cells from migrating throughout the scaffold (Fig. 9). MSCs have shown to have a strong attachment to fibrin by way of small binding domains, known as haptides, with the cell membrane, which is not found with other cell types (Xie et al., 2013a). The cellular gradient observed in collagen-GAG matrices showed a higher concentration at the seeding side with a steady amount of migration throughout the scaffold. In addition, the silicone layer component, opposite of the seeding side, creates a barrier so the cells cannot migrate completely through the scaffold. As collagen is the main component of the ECM it was expected that the cells are able to attach and distribute throughout this scaffold. Beyond their porosity, as both collagen and fibrin are dominant in the ECM, it is no surprise they exhibit a high cellular bond. Furthermore, AdMSCs isolated from lipoaspirates have shown a high affinity for binding to ECM proteins (Amos et al., 2008). Beyond that, AdMSCs seeded in collagen-GAG matrices exhibited the highest level of metabolic activity and lowest level of cytotoxicity on day one.

The fibrin and collagen-GAG matrices showed the best potential for achieving this sort of architecture. Furthermore, the fibrin and collagen-GAG matrices showed the highest amount of cell migration of the four scaffolds, although at different distributions, which could be attributed to differences in cellular adhesion and migration triggered by the material itself (Harley et al., 2008; Yasuda et al., 2010). Throughout the observation, the cells seeded on the collagen-GAG matrix exhibited the steadiest rate of proliferation and the lowest rate of cellular death indicating the most compatible relationship between cells and biomaterial.

5.1.1.3 Decellularized dermis

Although AdMSCs seeded onto the decellularized dermis were able to migrate through the material, a strong decrease in metabolic activity was seen shortly after seeding, indicating that it may not provide adequate room for the cells to thrive or may even induce cell death (Fig. 11). This might be particularly important for the decellularized dermis as it went through cell removal during preparation. The decellularized dermis utilized here, Strattice™, has been used successfully as an internally placed scaffold for treatment of subcostal hernia repair (King et al., 2013) and breast reconstruction

(Glasberg and Light, 2012; Pozner et al., 2013). Mirastschijski *et al.* have found that the decellularized dermis may be best suited for dermal wound beds that require a high mechanical load as in those previously mentioned (Mirastschijski et al., 2013). While the residual porosity does facilitate some AdMSC migration, the high mortality rate would not make this a suitable scaffold for a cell seeded dermal wound treatment. This high mortality rate may be due to residual chemicals as a result of the decellularization process that cannot be easily washed away before cell seeding. However, the low cellular infiltration that we observed *in vitro* agrees with previous data showing similar results after subcutaneous implantation of the scaffold in a rat model (Monteiro et al., 2013).

Although the metabolic activity increased over time in the decellularized dermis, despite the initial rate of cellular death, it seems to be the least compatible combination of the AdMSCs and biomaterial of the four examined. This may be a result of cells overcrowding due to tight porosity and could limit the amount of cells able to flourish. In addition, pore sizes in the decellularized dermis were not uniform in size enough for the cell-cell interaction necessary for the cells to thrive. Furthermore, the low metabolic activity observed over two weeks of seeding correlates with a high count of cell death only one day after seeding.

5.1.2 Scaffold-AdMSC secretion profile

During the first days after wounding, the release of paracrine factors is crucial for wound healing (Singer and Caplan, 2011). Independent of their differentiation capacity, MSCs have been shown to act as anti-inflammatory and immunoregulatory agents (Newman et al., 2009; Singer and Caplan, 2011), promote cell migration and proliferation, angiogenesis, and improve scarring (Maxson et al., 2012). The application of MSC seeded scaffolds to wounds could, therefore, be beneficial in all the three phases of wound healing: inflammation, proliferation, and tissue remodeling.

Although chitosan is the only material of the four scaffolds that is not found in the human body, it has been used successfully in wound healing treatments (Dai et al., 2011). It is surprising that the chitosan film lead to a significantly higher release of Serpin E1 than control cells and fibrin matrices. Serpin E1 is known to regulate extracellular matrix (ECM) remodeling (Providence et al., 2008), which is why a high level of expression from the collagen-GAG matrices was expected (Fig 12).

VEGF and PlGF work together to induce angiogenesis, endothelial cell growth, and promote cell proliferation and migration. VEGF expression is dependent on PlGF while the PlGF/VEGF heterodimer induces pathological angiogenesis (Blaber et al., 2012; Carmeliet et al., 2001; Tjwa et al., 2003). In general, the scaffolds had a significant effect in reducing VEGF and increasing PlGF expression relative to the two-dimensional culture (Fig. 12). While little variation of this effect was found between each scaffold, this may imply that the scaffold itself upregulates the angiogenic potential of AdMSCs.

An increase in IL-6 could accelerate wound healing by increased rates of angiogenesis and epithelial cell migration (Yew et al., 2011). The scaffold composition did not seem to affect the release of this cytokine except in the case of the collagen-GAG matrix where it was upregulated. IL-6 is known to induce collagen and GAG production (Duncan and Berman, 1991) and a similar increase in IL-6 can be seen with primary human dermal fibroblasts seeded on a collagen-GAG matrix (García-Gareta et al., 2013). IL-6 also functions in pro- and anti-inflammatory situations and is a major regulator of acute phase reactions, which indicates a wound-like stimulation *in vitro*. IL-8 had a much lower expression rate in the chitosan film and collagen-GAG matrices compared to the fibrin matrix, which was similar to the cell only control. Fibrin is known to induce IL-8 expression in human umbilical vein endothelial cells (HUVECs) (Qi et al., 1997) and a relatively high expression of IL-8 was found in a previous study utilizing primary human dermal fibroblasts on the fibrin matrix (García-Gareta et al., 2013). IL-6 has been linked to angiogenesis by increasing VEGF expression (Cohen et al., 1996) and IL-8 has been shown to upregulate VEGF in endothelial cells (Martin et al., 2009) and BMMSCs (Hou et al., 2014) via signaling pathways.

The cells released factors into the medium that contributed to increased angiogenesis. In particular, the conditioned medium from the collagen-GAG matrix showed no significant difference in small vessel convergence and growth with that of the VEGF positive control (Fig. 13). The medium from the scaffolds themselves did not differ from the vascular growth seen when using PBS indicating that the synergistic effects of the AdMSCs with the scaffolds was the main component in the increased rates of angiogenesis. The CAM offers an exceptional model, as there is no immune system, and the vascular networks are exposed.

These results are interesting as they show that scaffolds could not only be designed to harbor AdMSCs, but should be optimized to work synergistically with the cells in order to enhance the release of necessary and desirable factors to enhance wound healing by promoting angiogenesis, reducing healing time, and minimizing scar tissue.

The scaffolds evaluated for this work were selected due to their use in clinics worldwide. Integra® DRT was developed to mimic human skin and composed of a biodegradable bovine collagen-GAG to resemble the dermal layer and a silicone film protective layer as the epidermis. It is often used to treat severe burns and has been proven to reduce scar tissue (Campitiello et al., 2005; Dantzer et al., 2001; Moiemen et al., 2006). On top of the benefits it has alone, it was able to create a welcoming environment for the cells via porosity to allow for cell migration and viability throughout the material, to increase IL-6 production, while maintaining favorable levels of VEGF, Serpin E1, and PIGF *in vitro*, and revealed the highest amount of small vessel formation *in vivo*. Furthermore, the structure of the scaffold does not change, as with the fibrin matrix, which allows for more standardization of cell density. As a result, the collagen-GAG matrix was chosen to be further optimized in this work.

5.2 Influence of hypoxia and hypoxia-mimetic pre-conditioning of AdMSCs on pro-angiogenic protein expression *in vitro* and *in vivo*

The seeding density of the collagen-GAG scaffold was determined by way of the metabolic activity in regards to the cellular proliferation of AdMSCs over time. The concentration determined to be the most suitable in regards to quick and stable cellular growth without loss of activity overtime was 5×10^5 AdMSCs per 10 mm collagen-GAG disc (Fig. 14), equivalent to 6.4×10^5 cells per cm^2. This information could give insight into the optimal cellular density for larger scaffolds for translation into clinical application.

After determining the optimal seeding density, the AdMSCs were exposed to hypoxia and hypoxia-mimetic conditions by way of 1% O_2 and DFO at different concentrations. In order to control if the DFO was creating hypoxia-mimetic conditions, the level of HIF-1α was quantified from treated and

untreated cells (Fig. 15). While there was no difference in expression after 12 h between environmental hypoxia and cells exposed to 30 and 60 μM DFO, those exposed to 120 μM of DFO showed a higher amount of HIF-1α indicating that it is concentration dependent.

HIF-1α activity is suppressed in diabetics due to the high-glucose levels and, as a result, impairs wound healing (Thangarajah et al., 2010). Thangarajah *et al.* found that therapeutic doses of DFO could create HIF-1α activity and, therefore, the release of VEGF to improve angiogenesis (Thangarajah et al., 2010). Wang *et al.* showed that local injections of DFO enhanced healing in diabetic skin flaps in mice, similar to non-diabetic animals, through an increased production of HIF-1α and VEGF (Wang et al., 2014). Hou *et al.* also found that by treating HUVECs with DFO in diabetic rats that there was an increased level of angiogenesis and wound healing (Hou et al., 2013b). Furthermore, Zhang *et al.* found that irradiated mice treated with DFO showed increased healing and function of salivary glands (Zhang et al., 2014). Elevated HIF-1α levels lead to an upregulation of VEGF, as well as several other genes, such as erythropoietin, increased cell survival, and glycolysis (Semenza, 2007; Yuan et al., 2008), which would in turn lead to improved healing.

The release of VEGF triggers endothelial cells to migrate and proliferate in order to form new immature vessels (Coultas et al., 2005). *In vitro,* the highest release of VEGF was observed after 3 and 7 days when the cells were treated with 120 μM DFO compared to the normoxic treatment (Fig. 16A). The increase in VEGF release with 120 μM DFO treated cells correlates with the higher release of HIF-1α from the same cells. The addition of hypoxia and hypoxia-mimetic conditions enhanced levels of VEGF, which could also enhance MSC migration and, furthermore, VEGF has been shown to be the critical mediator for MSCs towards angiogenesis (Beckermann et al., 2008).

In vivo, the release of VEGF did not significantly differ between cells treated with normoxic and hypoxic conditions (Fig. 19A). The cells in hypoxic conditions may have undergone stress during the transplant by suddenly being exposed to normoxic conditions. As the environmental hypoxic effects would soon be lost and the measurement was taken 14 days after transplantation, a combination of cell stress, that may have led to cellular death, could lessen the effects of the pre-conditioning when compared to those from the cells exposed to normoxic conditioning. This would indicate that the cells

are altered from the sudden change in oxygen tension and make environmental hypoxia an unpredictable treatment. As DFO is taken up by cells the outcome would not be effected upon transplantation.

In wound healing, SDF-1α is responsible for recruiting MSCs and their release of growth factors to the injured tissue as well as increasing wound healing rates and neovascularization (Xu et al., 2013). The release of SDF-1α *in vitro* was significantly higher after 7 days when the AdMSCs were treated with DFO and was not concentration dependent (Fig. 16B). With environmental hypoxia the release was lower than cells exposed to normoxic conditions. Although it has been found that BMMSCs lose CXCR4, the receptor for SDF-1α (Potapova et al., 2008) *in vitro,* Najafi *et al.* found treating the cells with DFO could increase the expression of CXCR4 *in vitro* (Najafi and Sharifi, 2013). It is not surprising then that there was such a significantly high increase of SDF-1α *in vitro* from the AdMSCs treated with DFO, as CXCR4 is the receptor for SDF-1α. Furthermore, the release of SDF-1α was lower in cells treated with environmental hypoxia than those treated with normoxic conditions. Jing *et al*. also found a downregulation of SDF-1α with BMMSCs in hypoxic conditions (Jing et al., 2012), suggesting that oxygen tensions similar to their niche *in vitro* is not useful to the release chemotactic factors. On the other hand, there was no significant difference in SDF-1α expression between treatments *in vivo* (Fig 19B). Liu *et al*. found that hypoxia preconditioned MSCs had upregulated the expression of SDF-1α when compared to those treated in normoxic conditions (Liu et al., 2012). They also found in subsequent treatments that the differences in levels of SDF-1α peaked at 48 h and became comparable after 7 days (Liu et al., 2012). As the data mentioned here was analyzed 14 days after transplantation, further differences may be visible at earlier time points.

Without vascularization, transplanted cells will undergo apoptosis. Therefore, the transplanted cells need to be close to the damaged vasculature of a wound in order to survive (Sheridan et al., 2000). In the mouse model utilized, there was a visually higher density of neovascularization with hypoxic treatments than with normoxic treatments when analyzed after 14 days. Furthermore, there seems to be a higher instance of neovascularization with cells than with no cells at all. In the mouse model utilized in this research, the skin was removed and the scaffolds were placed over undamaged

muscle tissue, which is highly vascularized, this could have facilitated AdMSC survival and growth factor release. For chronic wound treatment in a patient, necrotic tissue and debris would need to be removed and the underlying tissue and muscle may provide enough vasculature for the transplanted AdMSCs to thrive. This analogy supports the use of this mouse model for chronic wound simulation.

5.3 *In vivo* inflammatory response of pre-conditioned AdMSCs

Inflammation is an important stage in wound healing and needs to occur for successful healing. Chronic wounds remain in a state of prolonged inflammation that could be due to both local and systemic defects (Eming et al., 2007). Interestingly, IL-12p70 was exhibited in small amounts from all treatments (Fig. 17). As IL-12p70 stimulates T cells to produce IFN-γ a cytokine activated by inflammation, which could reduce an occurrence of fibrosis (Bansal et al., 2014). Knockout IFN-γ and IL-10 mice exhibit increased epithelialization, angiogenesis, and collagen deposition resulting in increased wound closure (Eming et al., 2007; Ishida et al., 2004). Therefore, the lack of expression of these cytokines produce a desired effect but while IFN-γ is necessary to viral infections, it can be toxic against other infections (Trinchieri, 2010).

IL-6 can be either a pro- or anti-inflammatory cytokine (Scheller et al., 2011) but is crucial in wound healing by way of impaired angiogenesis, leukocyte recruitment, and collagen deposition (Lin et al., 2003). Furthermore, Lin *et al.* have demonstrated that IL-6 knockout mice have delayed wound healing (Lin et al., 2003). In addition, Gallucci *et al.* also found a decreased inflammatory response, reduced re-epithelialization, and reduced granulation tissue formation with these mice (Gallucci et al., 2000). MCP-1 induces endothelial cell migration and VEGF-mediated angiogenesis (Hong et al., 2005; Yamada et al., 2003). MCP-1 knockout mice experience delayed re-epithelialization, angiogenesis, and collagen synthesis (Low et al., 2001). The significantly high expression of IL-6 and MCP-1 from mice receiving the DFO treated cells (Fig. 17) indicates there is an increase in healing through inflammatory cytokine expression. TNF expression has been shown to be present in situations that inhibit (Eming et al., 2007) and enhance (Ashcroft et al., 2012; Daley et al., 2010) wound healing. Due to the expression of the other inflammatory cytokines in this work, it can be assumed that the TNF expression exhibited provides a favorable result. However, in elderly patients

an increased level of IL-6 and TNF can be associated with a decrease of necessary wound healing growth factors (Gould et al., 2014)

6. CONCLUSIONS AND OUTLOOK

In this work, a suitable delivery vehicle for AdMSCs to the wound that can secrete factors to facilitate healing was evaluated. AdMSCs in conjunction with the different scaffold types examined released angiogenic factors and chemokines necessary for wound healing. Although the decellularized dermis (Strattice™) is used in clinical settings, its lack of porosity and the poor environment it creates for the AdMSCs does not make it an ideal candidate for a cell seeded, topically applied wound treatment. Cells seeded on the chitosan film secreted factors that are helpful in wound healing although the scaffold lacked the capability to let cells migrate throughout, leaving a crowded film of cells at the seeding side which could be lost upon transplantation. While the addition of pores could improve this, the thickness and material would not offer an optimal delivery platform for AdMSCs. The ability for a scaffold to provide (i) an ideal environment for the cells to migrate, (ii) porosity that facilitates cell migration and crosstalk, and (iii) a biocompatible material are necessary to achieve proper healing *in vivo.* Through the investigative efforts, the collagen-GAG and fibrin matrices proved to have the best potential under the applied conditions as a platform for AdMSCs to enhance wound healing *in vitro.* The *in vivo* CAM data correlates with the *in vitro* data to further show the collagen-GAG and fibrin matrices are superior in working with the AdMSCs to promote angiogenesis and thus speed healing. Due to the more stable structure of the collagen-GAG matrix, it was utilized for further investigation.

Furthermore, this work set out to pre-condition the AdMSCs seeded scaffold *in vitro* at low oxygen tensions, as they exist in their niche, and hypoxia-mimetic conditions, with DFO, in order to maintain their angiogenic potential. The wound healing potential was assessed by the angiogenic potential and cytokine release via protein expression.

The stabilization of HIF-1α in order to increase VEGF production was obtained through DFO. Furthermore, the pattern of inflammation related factors matched the ones previously described to increase wound healing, further indicating DFO could be a promising alternative to environmentally initiated hypoxia making clinical translation easier. The inflammatory effects were evaluated on a systematic level. While these values were favorable for DFO treated cells, the local effects could also be examined to determine any possible differences. In addition, a more detailed analysis of the

interaction of the scaffolds and cells in the host environment by way of additional growth factor analysis at additional time points *in vivo* would be beneficial.

DFO has been used in clinical settings and should demonstrate a reasonably applicable wound healing treatment for wound healing for diabetics, the elderly, and immuno-impaired patients with the methods evaluated. With the right resources, the culture and expansion of AdMSCs in DFO may improve the angiogenic and wound healing potential by providing a more stable environment to the cells after isolation up until the point of transplantation. Although, the isolation and maintenance of the cells still remain an issue that needs to be handled in a laboratory setting in order to obtain a more homogeneous culture. Furthermore, additional animal experiments with those that have impaired healing such as elderly or diabetic animals at longer time points and larger animals, such as pigs, would be beneficial to see the effects after full wound healing. In addition, the development of a model that mimics chronic wounds more closely would be beneficial for future studies.

Although chronic wounds are a clinical issue where the methods for healing require more improvement, this study offers insights into the delivery of AdMSCs to injured tissue via a scaffold. Therefore, this data helps to develop new strategies for the treatment of other tissue defects that could benefit from cell-seeded scaffold healing, such as internal damages related to stroke, heart disease, or non-healing bone fractures.

References

Achilleos, A., and Trainor, P.A. (2012). Neural crest stem cells: discovery, properties and potential for therapy. Cell research *22*, 288-304.

Akpinar, G., Kasap, M., Aksoy, A., Duruksu, G., Gacar, G., and Karaoz, E. (2014). Phenotypic and proteomic characteristics of human dental pulp derived mesenchymal stem cells from a natal, an exfoliated deciduous, and an impacted third molar tooth. Stem Cells Int *2014*, 457059.

Amos, P.J., Bailey, A.M., Shang, H., Katz, A.J., Lawrence, M.B., and Peirce, S.M. (2008). Functional binding of human adipose-derived stromal cells: effects of extraction method and hypoxia pretreatment. Annals of plastic surgery *60*, 437-444.

Anthony, D.F., and Shiels, P.G. (2013). Exploiting paracrine mechanisms of tissue regeneration to repair damaged organs. Transplant Res *2*, 10.

Ashcroft, G.S., Jeong, M.J., Ashworth, J.J., Hardman, M., Jin, W., Moutsopoulos, N., Wild, T., McCartney-Francis, N., Sim, D., McGrady, G.*, et al.* (2012). Tumor necrosis factor-alpha (TNF-alpha) is a therapeutic target for impaired cutaneous wound healing. Wound repair and regeneration : official publication of the Wound Healing Society [and] the European Tissue Repair Society *20*, 38-49.

Atala, A., Kasper, F.K., and Mikos, A.G. (2012). Engineering complex tissues. Science translational medicine *4*, 160rv112.

Aust, L., Devlin, B., Foster, S.J., Halvorsen, Y.D., Hicok, K., du Laney, T., Sen, A., Willingmyre, G.D., and Gimble, J.M. (2004). Yield of human adipose-derived adult stem cells from liposuction aspirates. Cytotherapy *6*, 7-14.

Bansal, R., Prakash, J., De Ruiter, M., and Poelstra, K. (2014). Targeted recombinant fusion proteins of IFNgamma and mimetic IFNgamma with PDGFbetaR bicyclic peptide inhibits liver fibrogenesis in vivo. PLoS One *9*, e89878.

Baraniak, P.R., and McDevitt, T.C. (2010). Stem cell paracrine actions and tissue regeneration. Regen Med *5*, 121-143.

Barbash, I.M., Chouraqui, P., Baron, J., Feinberg, M.S., Etzion, S., Tessone, A., Miller, L., Guetta, E., Zipori, D., Kedes, L.H.*, et al.* (2003). Systemic delivery of bone marrow-derived mesenchymal stem cells to the infarcted myocardium: feasibility, cell migration, and body distribution. Circulation *108*, 863-868.

Baron, F., and Storb, R. (2012). Mesenchymal stromal cells: a new tool against graft-versus-host disease? Biology of blood and marrow transplantation : journal of the American Society for Blood and Marrow Transplantation *18*, 822-840.

Barrientos, S., Brem, H., Stojadinovic, O., and Tomic-Canic, M. (2014). Clinical application of growth factors and cytokines in wound healing. Wound repair and regeneration : official publication of the Wound Healing Society [and] the European Tissue Repair Society *22*, 569-578.

Bartolome, S., Dhillon, N.K., Buch, S., Casillan, A.J., Wood, J.G., and O'Brien-Ladner, A.R. (2009). Deferoxamine mimics the pattern of hypoxia-related injury at the microvasculature. Shock (Augusta, Ga) *31*, 481-485.

Basaran, U.N., Ayvaz, S., Aksu, B., Karaca, T., Cemek, M., Karaboga, I., Inan, M., Aksu, F., and Pul, M. (2013). Desferrioxamine reduces oxidative stress in the lung contusion. TheScientificWorldJournal *2013*, 376959.

Beckermann, B.M., Kallifatidis, G., Groth, A., Frommhold, D., Apel, A., Mattern, J., Salnikov, A.V., Moldenhauer, G., Wagner, W., Diehlmann, A.*, et al.* (2008). VEGF expression by mesenchymal stem cells contributes to angiogenesis in pancreatic carcinoma. British journal of cancer *99*, 622-631.

Bieback, K., Wuchter, P., Besser, D., Franke, W., Becker, M., Ott, M., Pacher, M., Ma, N., Stamm, C., Klüter, H.*, et al.* (2012). Mesenchymal stromal cells (MSCs): science and f(r)iction. J Mol Med *90*, 773-782.

Blaber, S.P., Webster, R.A., Hill, C.J., Breen, E.J., Kuah, D., Vesey, G., and Herbert, B.R. (2012). Analysis of in vitro secretion profiles from adipose-derived cell populations. J Transl Med *10*, 172.

Boquest, A.C., Shahdadfar, A., Fronsdal, K., Sigurjonsson, O., Tunheim, S.H., Collas, P., and Brinchmann, J.E. (2005). Isolation and transcription profiling of purified uncultured human stromal stem cells: alteration of gene expression after in vitro cell culture. Molecular biology of the cell *16*, 1131-1141.

Botusan, I.R., Sunkari, V.G., Savu, O., Catrina, A.I., Grunler, J., Lindberg, S., Pereira, T., Yla-Herttuala, S., Poellinger, L., Brismar, K.*, et al.* (2008). Stabilization of HIF-1alpha is critical to improve wound healing in diabetic mice. Proceedings of the National Academy of Sciences of the United States of America *105*, 19426-19431.

Bouffi, C., Bony, C., Courties, G., Jorgensen, C., and Noel, D. (2010). IL-6-dependent PGE2 secretion by mesenchymal stem cells inhibits local inflammation in experimental arthritis. PLoS One *5*, e14247.

Branch, M.J., Hashmani, K., Dhillon, P., Jones, D.R., Dua, H.S., and Hopkinson, A. (2012). Mesenchymal stem cells in the human corneal limbal stroma. Investigative ophthalmology & visual science *53*, 5109-5116.

Brem, H., Maggi, J., Nierman, D., Rolnitzky, L., Bell, D., Rennert, R., Golinko, M., Yan, A., Lyder, C., and Vladeck, B. (2010). High cost of stage IV pressure ulcers. American journal of surgery *200*, 473-477.

Broughton, G., Janis, J.E., and Attinger, C.E. (2006). The basic science of wound healing. Plast Reconstr Surg *117*, 12S-34S.

Brown, G. (2003). Long-term outcomes of full-thickness pressure ulcers: healing and mortality. Ostomy/wound management *49*, 42-50.

Burke, J.F., Yannas, I.V., Quinby, W.C., Jr., Bondoc, C.C., and Jung, W.K. (1981). Successful use of a physiologically acceptable artificial skin in the treatment of extensive burn injury. Annals of surgery *194*, 413-428.

Campitiello, E., Della Corte, A., Fattopace, A., D'Acunzi, D., and Canonico, S. (2005). The use of artificial dermis in the treatment of chronic and acute wounds: regeneration of dermis and wound healing. Acta bio-medica : Atenei Parmensis *76 Suppl 1*, 69-71.

Carmeliet, P., Moons, L., Luttun, A., Vincenti, V., Compernolle, V., De Mol, M., Wu, Y., Bono, F., Devy, L., Beck, H.*, et al.* (2001). Synergism between vascular endothelial growth factor and placental growth factor contributes to angiogenesis and plasma extravasation in pathological conditions. Nat Med *7*, 575-583.

Castilla, D.M., Liu, Z.J., and Velazquez, O.C. (2012). Oxygen: Implications for Wound Healing. Advances in wound care *1*, 225-230.

Chabannes, D., Hill, M., Merieau, E., Rossignol, J., Brion, R., Soulillou, J.P., Anegon, I., and Cuturi, M.C. (2007). A role for heme oxygenase-1 in the immunosuppressive effect of adult rat and human mesenchymal stem cells. Blood *110*, 3691-3694.

Chattopadhyay, S., and Raines, R.T. (2014). Review collagen-based biomaterials for wound healing. Biopolymers *101*, 821-833.

Chavakis, E., Urbich, C., and Dimmeler, S. (2008). Homing and engraftment of progenitor cells: a prerequisite for cell therapy. Journal of molecular and cellular cardiology *45*, 514-522.

Chen, G., Yue, A., Ruan, Z., Yin, Y., Wang, R., Ren, Y., and Zhu, L. (2014). Human Umbilical Cord-Derived Mesenchymal Stem Cells Do Not Undergo Malignant Transformation during Long-Term Culturing in Serum-Free Medium. PLoS ONE *9*, e98565.

Chen, H.T., Lee, M.J., Chen, C.H., Chuang, S.C., Chang, L.F., Ho, M.L., Hung, S.H., Fu, Y.C., Wang, Y.H., Wang, H.I.*, et al.* (2012). Proliferation and differentiation potential of human adipose-derived mesenchymal stem cells isolated from elderly patients with osteoporotic fractures. J Cell Mol Med *16*, 582-593.

Chen, L., Tredget, E.E., Wu, P.Y.G., and Wu, Y. (2008). Paracrine factors of mesenchymal stem cells recruit macrophages and endothelial lineage cells and enhance wound healing. PLoS One *3*, e1886.

Choi, J.S., Kim, J.D., Yoon, H.S., and Cho, Y.W. (2013). Full-thickness skin wound healing using human placenta-derived extracellular matrix containing bioactive molecules. Tissue Eng Part A *19*, 329-339.

Chow, D.C., Wenning, L.A., Miller, W.M., and Papoutsakis, E.T. (2001). Modeling pO(2) distributions in the bone marrow hematopoietic compartment. II. Modified Kroghian models. Biophys J *81*, 685-696.

Chung, H.M., Won, C.H., and Sung, J.H. (2009). Responses of adipose-derived stem cells during hypoxia: enhanced skin-regenerative potential. Expert Opin Biol Ther *9*, 1499-1508.

Cipolleschi, M.G., Dello Sbarba, P., and Olivotto, M. (1993). The role of hypoxia in the maintenance of hematopoietic stem cells. Blood *82*, 2031-2037.

Cohen, T., Nahari, D., Cerem, L.W., Neufeld, G., and Levi, B.Z. (1996). Interleukin 6 induces the expression of vascular endothelial growth factor. J Biol Chem *271*, 736-741.

Cohnheim, J. (1867). Über Entzündung und Eiterung. Virchows Archiv A: Pathology Pathologische Anatomie *40*, 1-79.

Collins, M.N., and Birkinshaw, C. (2013). Hyaluronic acid based scaffolds for tissue engineering--a review. Carbohydrate polymers *92*, 1262-1279.

Coultas, L., Chawengsaksophak, K., and Rossant, J. (2005). Endothelial cells and VEGF in vascular development. Nature *438*, 937-945.

Crandall, D.L., Hausman, G.J., and Kral, J.G. (1997). A review of the microcirculation of adipose tissue: anatomic, metabolic, and angiogenic perspectives. Microcirculation (New York, NY : 1994) *4*, 211-232.

da Silva Meirelles, L., Chagastelles, P.C., and Nardi, N.B. (2006). Mesenchymal stem cells reside in virtually all post-natal organs and tissues. Journal of cell science *119*, 2204-2213.

Dai, T., Tanaka, M., Huang, Y.-Y., and Hamblin, M.R. (2011). Chitosan preparations for wounds and burns: antimicrobial and wound-healing effects. Expert Rev Anti Infect Ther *9*, 857-879.

Daley, J.M., Brancato, S.K., Thomay, A.A., Reichner, J.S., and Albina, J.E. (2010). The phenotype of murine wound macrophages. Journal of leukocyte biology *87*, 59-67.

Dantzer, E., Queruel, P., Salinier, L., Palmier, B., and Quinot, J.F. (2001). [Integra, a new surgical alternative for the treatment of massive burns. Clinical evaluation of acute and reconstructive surgery: 39 cases]. Annales de chirurgie plastique et esthetique *46*, 173-189.

Dash, S.N., Dash, N.R., Guru, B., and Mohapatra, P.C. (2014). Towards reaching the target: clinical application of mesenchymal stem cells for diabetic foot ulcers. Rejuvenation Res *17*, 40-53.

Dings, J., Meixensberger, J., Jager, A., and Roosen, K. (1998). Clinical experience with 118 brain tissue oxygen partial pressure catheter probes. Neurosurgery *43*, 1082-1095.

Dohle, D.S., Pasa, S.D., Gustmann, S., Laub, M., Wissler, J.H., Jennissen, H.P., and Dünker, N. (2009). Chick ex ovo culture and ex ovo CAM assay: how it really works. J Vis Exp.

Dominici, M., Le Blanc, K., Mueller, I., Slaper-Cortenbach, I., Marini, F., Krause, D., Deans, R., Keating, A., Prockop, D., and Horwitz, E. (2006). Minimal criteria for defining multipotent mesenchymal stromal cells. The International Society for Cellular Therapy position statement. Cytotherapy *8*, 315-317.

Duncan, M.R., and Berman, B. (1991). Stimulation of collagen and glycosaminoglycan production in cultured human adult dermal fibroblasts by recombinant human interleukin 6. J Invest Dermatol *97*, 686-692.

Duscher, D., Neofytou, E., Wong, V.W., Maan, Z.N., Rennert, R.C., Inayathullah, M., Januszyk, M., Rodrigues, M., Malkovskiy, A.V., Whitmore, A.J.*, et al.* (2015). Transdermal deferoxamine prevents pressure-induced diabetic ulcers. Proceedings of the National Academy of Sciences of the United States of America *112*, 94-99.

Egaña, J.T., Condurache, A., Lohmeyer, J.A., Kremer, M., Stöckelhuber, B.M., Lavandero, S., and Machens, H.-G. (2009). Ex vivo method to visualize and quantify vascular networks in native and tissue engineered skin. Langenbecks Arch Surg *394*, 349-356.

Eliasson, P., and Jonsson, J.I. (2010). The hematopoietic stem cell niche: low in oxygen but a nice place to be. J Cell Physiol *222*, 17-22.

Eming, S.A., Werner, S., Bugnon, P., Wickenhauser, C., Siewe, L., Utermohlen, O., Davidson, J.M., Krieg, T., and Roers, A. (2007). Accelerated wound closure in mice deficient for interleukin-10. Am J Pathol *170*, 188-202.

Erecinska, M., and Silver, I.A. (2001). Tissue oxygen tension and brain sensitivity to hypoxia. Respiration physiology *128*, 263-276.

Falanga, V., Iwamoto, S., Chartier, M., Yufit, T., Butmarc, J., Kouttab, N., Shrayer, D., and Carson, P. (2007). Autologous Bone Marrow–Derived Cultured Mesenchymal Stem Cells Delivered in a Fibrin Spray Accelerate Healing in Murine and Human Cutaneous Wounds. Tissue Eng *13*, 1299-1312.

Friedenstein, A.J., Piatetzky, S., II, and Petrakova, K.V. (1966). Osteogenesis in transplants of bone marrow cells. Journal of embryology and experimental morphology *16*, 381-390.

Gallucci, R.M., Simeonova, P.P., Matheson, J.M., Kommineni, C., Guriel, J.L., Sugawara, T., and Luster, M.I. (2000). Impaired cutaneous wound healing in interleukin-6-deficient and immunosuppressed mice. FASEB journal : official publication of the Federation of American Societies for Experimental Biology *14*, 2525-2531.

García-Gareta, E., Ravindran, N., Sharma, V., Samizadeh, S., and Dye, J.F. (2013). A novel multiparameter in vitro model of three-dimensional cell ingress into scaffolds for dermal reconstruction to predict in vivo outcome. Biores Open Access *2*, 412-420.

Glasberg, S.B., and Light, D. (2012). AlloDerm and Strattice in breast reconstruction: a comparison and techniques for optimizing outcomes. Plast Reconstr Surg *129*, 1223-1233.

Golinko, M.S., Margolis, D.J., Tal, A., Hoffstad, O., Boulton, A.J., and Brem, H. (2009). Preliminary development of a diabetic foot ulcer database from a wound electronic medical record: a tool to decrease limb amputations. Wound repair and regeneration : official publication of the Wound Healing Society [and] the European Tissue Repair Society *17*, 657-665.

Gould, L., Abadir, P., Brem, H., Carter, M., Conner-Kerr, T., Davidson, J., DiPietro, L., Falanga, V., Fife, C., Gardner, S.*, et al.* (2014). Chronic Wound Repair and Healing in Older Adults: Current Status and Future Research. Wound repair and regeneration : official publication of the Wound Healing Society [and] the European Tissue Repair Society.

Grant, W.C., and Root, W.S. (1947). The relation of O2 in bone marrow blood to post-hemorrhagic erythropoiesis. The American journal of physiology *150*, 618-627.

Gurtner, G.C., Werner, S., Barrandon, Y., and Longaker, M.T. (2008). Wound repair and regeneration. Nature *453*, 314-321.

Halbleib, M., Skurk, T., de Luca, C., von Heimburg, D., and Hauner, H. (2003). Tissue engineering of white adipose tissue using hyaluronic acid-based scaffolds. I: in vitro differentiation of human adipocyte precursor cells on scaffolds. Biomaterials *24*, 3125-3132.

Harley, B.A.C., Kim, H.-D., Zaman, M.H., Yannas, I.V., Lauffenburger, D.A., and Gibson, L.J. (2008). Microarchitecture of three-dimensional scaffolds influences cell migration behavior via junction interactions. Biophys J *95*, 4013-4024.

Harris, L.J., Zhang, P., Abdollahi, H., Tarola, N.A., DiMatteo, C., McIlhenny, S.E., Tulenko, T.N., and DiMuzio, P.J. (2010). Availability of adipose-derived stem cells in patients undergoing vascular surgical procedures. The Journal of surgical research *163*, e105-112.

Harrison, J.S., Rameshwar, P., Chang, V., and Bandari, P. (2002). Oxygen saturation in the bone marrow of healthy volunteers. Blood *99*, 394.

Hirsila, M., Koivunen, P., Xu, L., Seeley, T., Kivirikko, K.I., and Myllyharju, J. (2005). Effect of desferrioxamine and metals on the hydroxylases in the oxygen sensing pathway. FASEB journal : official publication of the Federation of American Societies for Experimental Biology *19*, 1308-1310.

Hong, K.H., Ryu, J., and Han, K.H. (2005). Monocyte chemoattractant protein-1-induced angiogenesis is mediated by vascular endothelial growth factor-A. Blood *105*, 1405-1407.

Hopman, W.M., Harrison, M.B., Coo, H., Friedberg, E., Buchanan, M., and VanDenKerkhof, E.G. (2009). Associations between chronic disease, age and physical and mental health status. Chronic diseases in Canada *29*, 108-116.

Hou, C., Shen, L., Huang, Q., Mi, J., Wu, Y., Yang, M., Zeng, W., Li, L., Chen, W., and Zhu, C. (2013a). The effect of heme oxygenase-1 complexed with collagen on MSC performance in the treatment of diabetic ischemic ulcer. Biomaterials *34*, 112-120.

Hou, Y., Ryu, C.H., Jun, J.A., Kim, S.M., Jeong, C.H., and Jeun, S.S. (2014). IL-8 enhances the angiogenic potential of human bone marrow mesenchymal stem cells by increasing vascular endothelial growth factor. Cell biology international *38*, 1050-1059.

Hou, Z., Nie, C., Si, Z., and Ma, Y. (2013b). Deferoxamine enhances neovascularization and accelerates wound healing in diabetic rats via the accumulation of hypoxia-inducible factor-1alpha. Diabetes research and clinical practice *101*, 62-71.

Hung, S.C., Pochampally, R.R., Hsu, S.C., Sanchez, C., Chen, S.C., Spees, J., and Prockop, D.J. (2007). Short-term exposure of multipotent stromal cells to low oxygen increases their expression of CX3CR1 and CXCR4 and their engraftment in vivo. PLoS One *2*, e416.

Ishida, Y., Kondo, T., Takayasu, T., Iwakura, Y., and Mukaida, N. (2004). The essential involvement of cross-talk between IFN-gamma and TGF-beta in the skin wound-healing process. Journal of immunology (Baltimore, Md : 1950) *172*, 1848-1855.

Jackson, W.M., Nesti, L.J., and Tuan, R.S. (2012). Concise review: clinical translation of wound healing therapies based on mesenchymal stem cells. Stem Cells Transl Med *1*, 44-50.

Jing, D., Wobus, M., Poitz, D.M., Bornhauser, M., Ehninger, G., and Ordemann, R. (2012). Oxygen tension plays a critical role in the hematopoietic microenvironment in vitro. Haematologica *97*, 331-339.

Kang, S.K., Shin, I.S., Ko, M.S., Jo, J.Y., and Ra, J.C. (2012). Journey of Mesenchymal Stem Cells for Homing: Strategies to Enhance Efficacy and Safety of Stem Cell Therapy. Stem Cells Int *2012*, 1-11.

Kaufman, D.S. (2010). HIF hits Wnt in the stem cell niche. Nature cell biology *12*, 926-927.

Kim, E.J., Kim, N., and Cho, S.G. (2013). The potential use of mesenchymal stem cells in hematopoietic stem cell transplantation. Experimental & molecular medicine *45*, e2.

Kim, Y.M., Oh, S.H., Choi, J.S., Lee, S., Ra, J.C., Lee, J.H., and Lim, J.Y. (2014). Adipose-derived stem cell-containing hyaluronic acid/alginate hydrogel improves vocal fold wound healing. The Laryngoscope *124*, E64-72.

King, J., Hayes, J.D., and Richmond, B. (2013). Repair of giant subcostal hernia using porcine acellular dermal matrix (Strattice™) with bone anchors and pedicled omental flap coverage: a case report. J Med Case Rep *7*, 258.

Kirsner, R.S., Marston, W.A., Snyder, R.J., Lee, T.D., Cargill, D.I., Zhang, Y., Dickerson, J.E., Jr., and Slade, H.B. (2013). Durability of healing from spray-applied cell therapy with human allogeneic fibroblasts and keratinocytes for the treatment of chronic venous leg ulcers: a 6-month follow-up. Wound repair and regeneration : official publication of the Wound Healing Society [and] the European Tissue Repair Society *21*, 682-687.

Kofoed, H., Sjontoft, E., Siemssen, S.O., and Olesen, H.P. (1985). Bone marrow circulation after osteotomy. Blood flow, pO2, pCO2, and pressure studied in dogs. Acta Orthop Scand *56*, 400-403.

Lauto, A. (2009). Integration of extracellular matrix with chitosan adhesive film for sutureless tissue fixation. Lasers in surgery and medicine *41*, 366-371.

Lin, C.S., Lin, G., and Lue, T.F. (2012). Allogeneic and xenogeneic transplantation of adipose-derived stem cells in immunocompetent recipients without immunosuppressants. Stem Cells Dev *21*, 2770-2778.

Lin, C.S., Xin, Z.C., Deng, C.H., Ning, H., Lin, G., and Lue, T.F. (2010). Defining adipose tissue-derived stem cells in tissue and in culture. Histology and histopathology *25*, 807-815.

Lin, Z.Q., Kondo, T., Ishida, Y., Takayasu, T., and Mukaida, N. (2003). Essential involvement of IL-6 in the skin wound-healing process as evidenced by delayed wound healing in IL-6-deficient mice. Journal of leukocyte biology *73*, 713-721.

Liu, H., Liu, S., Li, Y., Wang, X., Xue, W., Ge, G., and Luo, X. (2012). The role of SDF-1-CXCR4/CXCR7 axis in the therapeutic effects of hypoxia-preconditioned mesenchymal stem cells for renal ischemia/reperfusion injury. PLoS One *7*, e34608.

Liu, H., Xue, W., Ge, G., Luo, X., Li, Y., Xiang, H., Ding, X., Tian, P., and Tian, X. (2010). Hypoxic preconditioning advances CXCR4 and CXCR7 expression by activating HIF-1alpha in MSCs. Biochem Biophys Res Commun *401*, 509-515.

Locke, M., Windsor, J., and Dunbar, P.R. (2009). Human adipose-derived stem cells: isolation, characterization and applications in surgery. ANZ Journal of Surgery *79*, 235-244.

Low, Q.E., Drugea, I.A., Duffner, L.A., Quinn, D.G., Cook, D.N., Rollins, B.J., Kovacs, E.J., and DiPietro, L.A. (2001). Wound healing in MIP-1alpha(-/-) and MCP-1(-/-) mice. Am J Pathol *159*, 457-463.

Ma, S., Xie, N., Li, W., Yuan, B., Shi, Y., and Wang, Y. (2014). Immunobiology of mesenchymal stem cells. Cell Death Differ *21*, 216-225.

Ma, T., Grayson, W.L., Fröhlich, M., and Vunjak-Novakovic, G. (2009). Hypoxia and Stem Cell-Based Engineering of Mesenchymal Tissues. Biotechnol Prog *25*, 32-42.

Martin, D., Galisteo, R., and Gutkind, J.S. (2009). CXCL8/IL8 stimulates vascular endothelial growth factor (VEGF) expression and the autocrine activation of VEGFR2 in endothelial cells by activating NFkappaB through the CBM (Carma3/Bcl10/Malt1) complex. J Biol Chem *284*, 6038-6042.

Matsumoto, A., Matsumoto, S., Sowers, A.L., Koscielniak, J.W., Trigg, N.J., Kuppusamy, P., Mitchell, J.B., Subramanian, S., Krishna, M.C., and Matsumoto, K. (2005). Absolute oxygen tension (pO(2)) in murine fatty and muscle tissue as determined by EPR. Magnetic resonance in medicine : official journal of the Society of Magnetic Resonance in Medicine / Society of Magnetic Resonance in Medicine *54*, 1530-1535.

Maxson, S., Lopez, E.A., Yoo, D., Danilkovitch-Miagkova, A., and Leroux, M.A. (2012). Concise review: role of mesenchymal stem cells in wound repair. Stem Cells Transl Med *1*, 142-149.

Mirastschijski, U., Kerzel, C., Schnabel, R., Strauss, S., and Breuing, K.-H. (2013). Complete horizontal skin cell resurfacing and delayed vertical cell infiltration into porcine reconstructive tissue matrix compared to bovine collagen matrix and human dermis. Plast Reconstr Surg *132*, 861-869.

Mirsaidi, A., Kleinhans, K.N., Rimann, M., Tiaden, A.N., Stauber, M., Rudolph, K.L., and Richards, P.J. (2012). Telomere length, telomerase activity and osteogenic differentiation are maintained in adipose-derived stromal cells from senile osteoporotic SAMP6 mice. J Tissue Eng and Regen Med *6*, 378-390.

Mitchell, J.A., and Yochim, J.M. (1968). Intrauterine oxygen tension during the estrous cycle in the rat: its relation to uterine respiration and vascular activity. Endocrinology *83*, 701-705.

Mizuno, H., Tobita, M., and Uysal, A.C. (2012). Concise Review: Adipose-Derived Stem Cells as a Novel Tool for Future Regenerative Medicine. Stem Cells *30*, 804-810.

Mohyeldin, A., Garzón-Muvdi, T., and Quiñones-Hinojosa, A. (2010). Oxygen in Stem Cell Biology: A Critical Component of the Stem Cell Niche. Cell Stem Cell *7*, 150-161.

Moiemen, N.S., Vlachou, E., Staiano, J.J., Thawy, Y., and Frame, J.D. (2006). Reconstructive surgery with Integra dermal regeneration template: histologic study, clinical evaluation, and current practice. Plast Reconstr Surg *117*, 160s-174s.

Monteiro, G.A., Rodriguez, N.L., Delossantos, A.I., and Wagner, C.T. (2013). Short-term in vivo biological and mechanical remodeling of porcine acellular dermal matrices. J Tissue Eng *4*, 2041731413490182.

Moulik, P.K., Mtonga, R., and Gill, G.V. (2003). Amputation and mortality in new-onset diabetic foot ulcers stratified by etiology. Diabetes care *26*, 491-494.

Muscari, C., Giordano, E., Bonafe, F., Govoni, M., Pasini, A., and Guarnieri, C. (2013). Priming adult stem cells by hypoxic pretreatments for applications in regenerative medicine. J Biomed Sci *20*, 63.

Najafi, R., and Sharifi, A.M. (2013). Deferoxamine preconditioning potentiates mesenchymal stem cell homing in vitro and in streptozotocin-diabetic rats. Expert Opin Biol Ther *13*, 959-972.

Newman, R.E., Yoo, D., LeRoux, M.A., and Danilkovitch-Miagkova, A. (2009). Treatment of inflammatory diseases with mesenchymal stem cells. Inflamm Allergy Drug Targets *8*, 110-123.

Ogawa, R. (2006). The importance of adipose-derived stem cells and vascularized tissue regeneration in the field of tissue transplantation. Current stem cell research & therapy *1*, 13-20.

Panchision, D.M. (2009). The role of oxygen in regulating neural stem cells in development and disease. J Cell Physiol *220*, 562-568.

Pasarica, M., Sereda, O.R., Redman, L.M., Albarado, D.C., Hymel, D.T., Roan, L.E., Rood, J.C., Burk, D.H., and Smith, S.R. (2009). Reduced adipose tissue oxygenation in human obesity: evidence for rarefaction, macrophage chemotaxis, and inflammation without an angiogenic response. Diabetes *58*, 718-725.

Pawitan, J. (2011). Future Research in Adipose Stem Cell Engineering. In Adipose Stem Cells and Regenerative Medicine, Y.-G. Illouz, and A. Sterodimas, eds. (Springer Berlin Heidelberg), pp. 257-272.

Pittenger, M.F. (1999). Multilineage Potential of Adult Human Mesenchymal Stem Cells. Science *284*, 143-147.

Potapova, I.A., Brink, P.R., Cohen, I.S., and Doronin, S.V. (2008). Culturing of human mesenchymal stem cells as three-dimensional aggregates induces functional expression of CXCR4 that regulates adhesion to endothelial cells. J Biol Chem *283*, 13100-13107.

Potier, E., Ferreira, E., Dennler, S., Mauviel, A., Oudina, K., Logeart-Avramoglou, D., and Petite, H. (2008). Desferrioxamine-driven upregulation of angiogenic factor expression by human bone marrow stromal cells. J Tissue Eng Regen Med *2*, 272-278.

Pouyssegur, J., Dayan, F., and Mazure, N.M. (2006). Hypoxia signalling in cancer and approaches to enforce tumour regression. Nature *441*, 437-443.

Pozner, J.N., White, J.B., and Newman, M.I. (2013). Use of porcine acellular dermal matrix in revisionary cosmetic breast augmentation. Aesthet Surg J *33*, 681-690.

Providence, K.M., Higgins, S.P., Mullen, A., Battista, A., Samarakoon, R., Higgins, C.E., Wilkins-Port, C.E., and Higgins, P.J. (2008). SERPINE1 (PAI-1) is deposited into keratinocyte migration "trails" and required for optimal monolayer wound repair. Arch Dermatol Res *300*, 303-310.

PTEI (2014). Scaffold-Guided Methods.

Qi, J., Goralnick, S., and Kreutzer, D.L. (1997). Fibrin regulation of interleukin-8 gene expression in human vascular endothelial cells. Blood *90*, 3595-3602.

Reagan, M.R., and Kaplan, D.L. (2011). Concise Review: Mesenchymal Stem Cell Tumor-Homing: Detection Methods in Disease Model Systems. Stem Cells *29*, 920-927.

Ren, G., Zhang, L., Zhao, X., Xu, G., Zhang, Y., Roberts, A.I., Zhao, R.C., and Shi, Y. (2008). Mesenchymal stem cell-mediated immunosuppression occurs via concerted action of chemokines and nitric oxide. Cell Stem Cell *2*, 141-150.

Ribatti, D., Nico, B., Vacca, A., and Presta, M. (2006). The gelatin sponge-chorioallantoic membrane assay. Nat Protoc *1*, 85-91.

Rosova, I., Dao, M., Capoccia, B., Link, D., and Nolta, J.A. (2008). Hypoxic preconditioning results in increased motility and improved therapeutic potential of human mesenchymal stem cells. Stem Cells *26*, 2173-2182.

Sato, K., Ozaki, K., Oh, I., Meguro, A., Hatanaka, K., Nagai, T., Muroi, K., and Ozawa, K. (2007). Nitric oxide plays a critical role in suppression of T-cell proliferation by mesenchymal stem cells. Blood *109*, 228-234.

Scheller, J., Chalaris, A., Schmidt-Arras, D., and Rose-John, S. (2011). The pro- and anti-inflammatory properties of the cytokine interleukin-6. Biochimica et biophysica acta *1813*, 878-888.

Schioppa, T., Uranchimeg, B., Saccani, A., Biswas, S.K., Doni, A., Rapisarda, A., Bernasconi, S., Saccani, S., Nebuloni, M., Vago, L.*, et al.* (2003). Regulation of the chemokine receptor CXCR4 by hypoxia. J Exp Med *198*, 1391-1402.

Schneider, C.A., Rasband, W.S., and Eliceiri, K.W. (2012). NIH Image to ImageJ: 25 years of image analysis. Nat Methods *9*, 671-675.

Schofield, R. (1978). The relationship between the spleen colony-forming cell and the haemopoietic stem cell. Blood cells *4*, 7-25.

Seidlits, S.K., Drinnan, C.T., Petersen, R.R., Shear, J.B., Suggs, L.J., and Schmidt, C.E. (2011). Fibronectin-hyaluronic acid composite hydrogels for three-dimensional endothelial cell culture. Acta Biomater *7*, 2401-2409.

Selmani, Z., Naji, A., Zidi, I., Favier, B., Gaiffe, E., Obert, L., Borg, C., Saas, P., Tiberghien, P., Rouas-Freiss, N.*, et al.* (2008). Human leukocyte antigen-G5 secretion by human mesenchymal stem cells is required to suppress T lymphocyte and natural killer function and to induce CD4+CD25highFOXP3+ regulatory T cells. Stem Cells *26*, 212-222.

Semenza, G.L. (2007). Oxygen-dependent regulation of mitochondrial respiration by hypoxia-inducible factor 1. The Biochemical journal *405*, 1-9.

Sheridan, M.H., Shea, L.D., Peters, M.C., and Mooney, D.J. (2000). Bioabsorbable polymer scaffolds for tissue engineering capable of sustained growth factor delivery. Journal of controlled release : official journal of the Controlled Release Society *64*, 91-102.

Shin, L., and Peterson, D.A. (2013). Human mesenchymal stem cell grafts enhance normal and impaired wound healing by recruiting existing endogenous tissue stem/progenitor cells. Stem Cells Transl Med *2*, 33-42.

Singer, N.G., and Caplan, A.I. (2011). Mesenchymal stem cells: mechanisms of inflammation. Annu Rev Pathol *6*, 457-478.

Spaggiari, G.M., Capobianco, A., Abdelrazik, H., Becchetti, F., Mingari, M.C., and Moretta, L. (2008). Mesenchymal stem cells inhibit natural killer-cell proliferation, cytotoxicity, and cytokine production: role of indoleamine 2,3-dioxygenase and prostaglandin E2. Blood *111*, 1327-1333.

Steigman, S.A., and Fauza, D.O. (2007). Isolation of mesenchymal stem cells from amniotic fluid and placenta. Current protocols in stem cell biology *Chapter 1*, Unit 1E.2.

Strem, B.M., Hicok, K.C., Zhu, M., Wulur, I., Alfonso, Z., Schreiber, R.E., Fraser, J.K., and Hedrick, M.H. (2005). Multipotential differentiation of adipose tissue-derived stem cells. The Keio journal of medicine *54*, 132-141.

Sun, W.Q., Xu, H., Sandor, M., and Lombardi, J. (2013). Process-induced extracellular matrix alterations affect the mechanisms of soft tissue repair and regeneration. J Tissue Eng *4*, 2041731413505305.

Takubo, K., Goda, N., Yamada, W., Iriuchishima, H., Ikeda, E., Kubota, Y., Shima, H., Johnson, R.S., Hirao, A., Suematsu, M.*, et al.* (2010). Regulation of the HIF-1alpha level is essential for hematopoietic stem cells. Cell Stem Cell *7*, 391-402.

Thangarajah, H., Vial, I.N., Grogan, R.H., Yao, D., Shi, Y., Januszyk, M., Galiano, R.D., Chang, E.I., Galvez, M.G., Glotzbach, J.P.*, et al.* (2010). HIF-1alpha dysfunction in diabetes. Cell cycle (Georgetown, Tex) *9*, 75-79.

Tholpady, S.S., Llull, R., Ogle, R.C., Rubin, J.P., Futrell, J.W., and Katz, A.J. (2006). Adipose tissue: stem cells and beyond. Clinics in plastic surgery *33*, 55-62, vi.

Tjwa, M., Luttun, A., Autiero, M., and Carmeliet, P. (2003). VEGF and PlGF: two pleiotropic growth factors with distinct roles in development and homeostasis. Cell Tissue Res *314*, 5-14.

Trinchieri, G. (2010). Type I interferon: friend or foe? J Exp Med *207*, 2053-2063.

Tully-Dartez, S., Cardenas, H.E., and Sit, P.-F.S. (2010). Pore characteristics of chitosan scaffolds studied by electrochemical impedance spectroscopy. Tissue Eng Part C Methods *16*, 339-345.

Wang, C., Cai, Y., Zhang, Y., Xiong, Z., Li, G., and Cui, L. (2014). Local injection of deferoxamine improves neovascularization in ischemic diabetic random flap by increasing HIF-1alpha and VEGF expression. PLoS One *9*, e100818.

Xie, M.W., Gorodetsky, R., Micewicz, E.D., Mackenzie, N.C., Gaberman, E., Levdansky, L., and McBride, W.H. (2013a). Marrow-derived stromal cell delivery on fibrin microbeads can correct radiation-induced wound-healing deficits. J Invest Dermatol *133*, 553-561.

Xie, M.W., Gorodetsky, R., Micewicz, E.D., Micevicz, E.D., Mackenzie, N.C., Gaberman, E., Levdansky, L., and McBride, W.H. (2013b). Marrow-derived stromal cell delivery on fibrin microbeads can correct radiation-induced wound-healing deficits. J Invest Dermatol *133*, 553-561.

Xing, Y., Lv, A., Wang, L., Yan, X., Zhao, W., and Cao, F. (2012). Engineered myocardial tissues constructed in vivo using cardiomyocyte-like cells derived from bone marrow mesenchymal stem cells in rats. J Biomed Sci *19*, 6.

Xu, S., and Chisholm, A.D. (2014). C. elegans epidermal wounding induces a mitochondrial ROS burst that promotes wound repair. Developmental cell *31*, 48-60.

Xu, X., Zhu, F., Zhang, M., Zeng, D., Luo, D., Liu, G., Cui, W., Wang, S., Guo, W., Xing, W.*, et al.* (2013). Stromal cell-derived factor-1 enhances wound healing through recruiting bone marrow-derived mesenchymal stem cells to the wound area and promoting neovascularization. Cells Tissues Organs *197*, 103-113.

Yamada, M., Kim, S., Egashira, K., Takeya, M., Ikeda, T., Mimura, O., and Iwao, H. (2003). Molecular mechanism and role of endothelial monocyte chemoattractant protein-1 induction by vascular endothelial growth factor. Arteriosclerosis, thrombosis, and vascular biology *23*, 1996-2001.

Yamamoto, Y., Fujita, M., Tanaka, Y., Kojima, I., Kanatani, Y., Ishihara, M., and Tachibana, S. (2013). Low oxygen tension enhances proliferation and maintains stemness of adipose tissue-derived stromal cells. Biores Open Access *2*, 199-205.

Yang, H.M., Sung, J.H., Choi, Y.S., Lee, H.J., Roh, C.R., Kim, J., Shin, M., Song, S., Kwon, C.H., Joh, J.W.*, et al.* (2012). Enhancement of the immunosuppressive effect of human adipose tissue-derived mesenchymal stromal cells through HLA-G1 expression. Cytotherapy *14*, 70-79.

Yasuda, H., Kuroda, S., Shichinohe, H., Kamei, S., Kawamura, R., and Iwasaki, Y. (2010). Effect of biodegradable fibrin scaffold on survival, migration, and differentiation of transplanted bone marrow stromal cells after cortical injury in rats. J Neurosurg *112*, 336-344.

Yew, T.-L., Hung, Y.-T., Li, H.-Y., Chen, H.-W., Chen, L.-L., Tsai, K.-S., Chiou, S.-H., Chao, K.-C., Huang, T.-F., Chen, H.-L.*, et al.* (2011). Enhancement of wound healing by human multipotent stromal cell conditioned medium: the paracrine factors and p38 MAPK activation. Cell Transplant *20*, 693-706.

Young, C., Jarrell, B.E., Hoying, J.B., and Williams, S.K. (1992). A porcine model for adipose tissue-derived endothelial cell transplantation. Cell Transplant *1*, 293-298.

Yu, S.P., Wei, Z., and Wei, L. (2013). Preconditioning strategy in stem cell transplantation therapy. Translational stroke research *4*, 76-88.

Yuan, G., Nanduri, J., Khan, S., Semenza, G.L., and Prabhakar, N.R. (2008). Induction of HIF-1alpha expression by intermittent hypoxia: involvement of NADPH oxidase, Ca2+ signaling, prolyl hydroxylases, and mTOR. J Cell Physiol *217*, 674-685.

Yukawa, H., Watanabe, M., Kaji, N., Okamoto, Y., Tokeshi, M., Miyamoto, Y., Noguchi, H., Baba, Y., and Hayashi, S. (2012). Monitoring transplanted adipose tissue-derived stem cells combined with heparin in the liver by fluorescence imaging using quantum dots. Biomaterials *33*, 2177-2186.

Zagorska, A., and Dulak, J. (2004). HIF-1: the knowns and unknowns of hypoxia sensing. Acta biochimica Polonica *51*, 563-585.

Zhang, J., Cui, L., Xu, M., and Zheng, Y. (2014). Restoring the Secretory Function of Irradiation-Damaged Salivary Gland by Administrating Deferoxamine in Mice. PLoS One *9*, e113721.

Zhao, D., Najbauer, J., Garcia, E., Metz, M.Z., Gutova, M., Glackin, C.A., Kim, S.U., and Aboody, K.S. (2008). Neural stem cell tropism to glioma: critical role of tumor hypoxia. Molecular cancer research : MCR *6*, 1819-1829.

Zomorodian, E., and Baghaban Eslaminejad, M. (2012). Mesenchymal stem cells as a potent cell source for bone regeneration. Stem Cells Int *2012*, 980353.

Zuk, P.A., Zhu, M., Ashjian, P., De Ugarte, D.A., Huang, J.I., Mizuno, H., Alfonso, Z.C., Fraser, J.K., Benhaim, P., and Hedrick, M.H. (2002). Human Adipose Tissue Is a Source of Multipotent Stem Cells. Mol Biol Cell *13*, 4279-4295.

Presentation of results

PUBLICATIONS

2015 **Wahl EA**, Rosado-Balmayor E, Machens HG, Egaña JT. VEGF released by deferoxamine preconditioned mesenchymal stem cells seeded on collagen-GAG substrates enhances neovascularization. **Manuscript in preparation**.

2015 **Wahl EA**, Fierro FA, Peavy TR, Hopfner U, Dye JF, Machens HG, Egaña JT, Schenck TL. Evaluation of Scaffolds for the Delivery of Mesenchymal Stem Cells to Wounds. **submitted**

2014 Reckhenrich AK, Kirsch BM, **Wahl EA**, Schenck TL, Rezaeian F, Harder Y, Foehr P, Machens HG, Egaña JT. Surgical sutures filled with adipose-derived stem cells promote wound healing. PLoS One. 9(3):e91169.

CONFERENCES

Poster Presentations

2014 VEGF released by deferoxamine preconditioned mesenchymal stem cells seeded on collagen-GAG substrates enhances wound healing
EMBO Conference – Stem Cells in Cancer and Regenerative Medicine
Heidelberg, Germany, October 9-12

2014 Evaluation of Scaffolds for the Delivery of Mesenchymal Stem Cells *In Vivo*
EMBO Conference – Stem Cells in Cancer and Regenerative Medicine
Heidelberg, Germany, October 9-12

2014 Evaluation of Scaffolds for the Delivery of Mesenchymal Stem Cells *In Vivo*
FEBS-EMBO (Federation of European Biochemical Societies – European Molecular Biology Organization)
Paris, France, August 31 – September 4

2014 Evaluation of Scaffolds for the Delivery of Mesenchymal Stem Cells *In Vivo*
<interact>
Munich, Germany, February 27-28

2013 *In Vitro* Evaluation of Scaffolds for the Delivery of Mesenchymal Stromal Cells *In Vivo*
TERMIS-EU (Tissue Engineering & Regenerative Medicine International Society)
Istanbul, Turkey, June 17-20

2012 Stem Cell-Seeded Scaffolds for Improving Tissue Regeneration In Vivo
EMBO
Nice, France, September 22-25

Acknowledgments

I would like to thank my thesis advisory committee, Prof. Hans-Günther Machens, Prof. Hans Hauner, and Dr. J. Tomás Egaña for their feedback on my research. Furthermore, I would like to thank our collaborators Thomas Peavey, Fernando Fierro, and Julian Dye for their contributions and the lab technicians Dibora Tibebu and Ursula Hopfner for keeping the lab intact. A big thank you goes to the TUM Graduate School for the various educational opportunities offered and the Medical Graduate School for their support to my many inquiries.

Mostly, I would like to thank my son and my rock, Graham, who kept me smiling through everything while helping me to realize how strong I can be and Mathias Labs who helped me through the hard times and carried me through the even rougher times. In addition, my brother Josh who helped me to maintain an artistic eye when making figures and my brother Jason who reminded me how important being able to communicate science is and what it all means to the public, up until his last days. A thank you to my dad who always believed in me and told me not give up throughout my life and my mom for crossing the ocean to lend a hand.